TOWARDS A COMPREHENSIVE SCALING LAW OF MIXTURE-OF-EXPERTS

Anonymous authors
Paper under double-blind review

ABSTRACT

Mixture-of-Experts (MoE) models have become the consensus approach for enabling parameter-efficient scaling and cost-effective deployment in large language models. However, existing scaling laws for dense models are inapplicable to MoE models, which stems from three critical challenges: the multiplicity of influencing factors, their intricate coupling relationships and the non-monotonic nature of their performance impacts. They collectively necessitate a fine-grained investigation into MoE-specific scaling laws. In this work, we perform a systematic decomposition of MoE settings, identifying five key factors that influence model performance from both size and structural perspectives (data size (D), total model size (N), activated model size (N_a), number of active experts (G) and the ratio of shared experts (S)). Specifically, we design 450 controlled experiments to characterize their marginal effects, ultimately constructing a comprehensive and precise joint MoE scaling law that considers all essential factors. Furthermore, we derive the theoretically optimal and practically efficiency-aware optimal configurations for G, S and N_a/N with detailed analyses. Our results demonstrate that the optimal settings for G and S are independent of both the model architecture and data size. With the scaling of N, the optimal activation parameter ratio of N_a/N becomes sparser. Our proposed MoE scaling law could function as an accurate and insightful guidance to facilitate future MoE model design and training.

1 INTRODUCTION

Large language models (LLMs) have been widely verified and utilized in our daily lives. It is impressive and lucky to discover that LLMs can continuously expand its ability boundaries with increasing model and training data sizes. The scaling laws of LLMs (Kaplan et al., 2020; Hoffmann et al., 2022; Sun et al., 2025), which could predict the model loss based on crucial factors (e.g., data/model sizes) before training, shed lights on the promising way of wisely selecting appropriate model structures and settings before experiments and continuously enhancing the ability of LLMs under given training budget or environment constraints. Recently, **Mixture-of-Experts (MoE)** becomes one of the mainstream structures broadly used in powerful industry-level LLMs (Dubey et al., 2024; Liu et al., 2024; Sun et al., 2024; Liu et al., 2025; Qwen Team et al., 2025; OpenAI et al., 2025). Different from the original dense architecture that involves all parameters in the forward process, MoE often adopts multiple experts (e.g., FFNs) with a router to automatically select which experts should be activated for the current token. The sparse activation of experts in MoE could largely benefit from increasing total model sizes while maintaining efficient model inference.

With the thriving in efficient LLMs, lots of efforts have been dedicated to MoE architectures. The shared expert is proposed to capture general knowledge robustly (Dai et al., 2024; Sun et al., 2024). We also notice the trend of increasing (activated and total) expert numbers (Kimi et al., 2025; Liu et al., 2024; OpenAI et al., 2025). In this case, existing scaling laws of either dense models (Kaplan et al., 2020; Hoffmann et al., 2022) or MoE models (Krajewski et al., 2024; Wang et al., 2024b) cannot perfectly predict the model performance under the updated popular MoE structures and settings. The community urgently requires a new MoE scaling law to accurately guide model training.

To comprehensively explore the central factors of MoE models that largely impact the model performance, we first take the classical factors of **data size** (D) and **total model size** (N) also marked in dense scaling laws into consideration. Besides, the **activated model size** (N_a) functioning in the

forward process is essential in MoE models. For the expert aspect, we note the **number of activated experts** G as another essential factor (N_a and G collaboratively determine the expert size). Moreover, the **ratio of shared experts in activated experts** (S) is also modeled (S and G collaboratively set the specific numbers of shared and routed experts). We attempt to build our scaling laws of MoE based on the above five factors. The challenges mainly locate in three aspects: (a) our MoE scaling law considers more comprehensive factors D, N, N_a, G, S compared to existing scaling laws. (b) Our preliminary experiments imply that some factors have a non-monotonic impact on loss, which are more challenging to fit. (c) There exists mutual coupling relationships among these factors, which multiplies the challenges of constructing the final joint scaling law.

To accomplish our MoE scaling laws, we first select a reasonable and wider parameter range for the five essential factors D, N, N_a, G, S and then conduct experiments 450 to record the corresponding MoE losses of different parameter settings. Based on these experimental results, we first decide the basic scaling law formation with the fundamental D, N factors following Hoffmann et al. (2022). Next, we discover the marginal effects of N_a, G, S respectively, whose impacts on model losses are surprisingly non-monotonic and are coupled to other factors. Finally, we obtain the joint MoE scaling laws formulated as follows:

$$L(N, D, N_a, G, S) = (eG + \frac{f}{G} + mS^2 + nS) * (\frac{1}{N^\alpha} + \frac{k}{N_a^\alpha} + h\frac{N_a}{N}) + \frac{a}{N^\alpha} + \frac{b}{D^\beta} + \frac{c}{N_a^\alpha} + \epsilon. \quad (1)$$

which could satisfactorily predict MoE models' losses with larger data/model sizes (e.g., up to 9B total model size and 100B trained tokens) and different MoE settings (e.g., up to 256 experts, 20 activated experts and 70% ratio of shared experts).

Based on our MoE scaling laws, we conduct in-depth analyses and discover the following implications: (a) ***the optimal number of activated experts is around 7*** for real-world classical MoE settings considering its effectiveness. (b) ***Too dense/sparse MoE structures are not performance-optimal***. The $20\% \sim 43\%$ activated parameter ratios (N_a/N) are theoretical optimal for N from 1T to 20B. Considering the cost, the practical efficiency-aware optimal ratios range from $5\% \sim 9\%$. (c) ***The existence of shared expert is essential***, while the best ratio S of shared experts to all activated experts ranges from $13\% \sim 31\%$ with marginal loss disturbances. We are confident that our MoE scaling laws with the above observations and insights could provide a more comprehensive understanding and more accurate performance prediction of MoE models with different settings, looking forward to facilitate LLM community in future MoE model design and training.

2 PRELIMINARY

2.1 MOE ARCHITECTURE

The Mixture-of-Experts (MoE) architecture modifies standard Transformer by replacing the dense Feed-Forward Networks (FFNs) with a set of independent experts, where each expert is usually an FFN of the same size (Fedus et al., 2022; Zhou et al., 2022; Jiang et al., 2024). Typically, for each token, the router selects and activates only a small subset of these experts. This design allows model size to grow by adding experts, while keeping the computational cost nearly unchanged. This makes it possible to scale models to very large sizes without a proportional increase in cost. Considering the trend of training-/inference- efficient LLM, MoE has become a mainstream and effective framework for building industry-level LLMs balancing model performance and computational efficiency.

2.2 EXISTING SCALING LAWS OF LLMS

Scaling Laws of Dense LLM. Scaling laws describe the relationship between key factors such as total model size N, data size D and the loss L. Classical scaling laws include the Chinchilla scaling law (Hoffmann et al., 2022), which states that L follows a power-law dependence on N and D, written as $L(N, D) = a/N^\alpha + b/D^\beta + \epsilon$. It consists of three terms: the first and second terms capture the limitations imposed by finite model size and finite data size, respectively. The last term, ϵ, represents the irreducible error that arises from the inherent uncertainty in the training data.

Scaling Laws for MoE. Unlike dense models, MoE introduces new structures with additional factors (e.g., the activated model size, the number of activated experts, the ratio of shared experts, etc),

whose effects on model loss are non-monotonic and often interdependent. Existing scaling laws for dense models are insufficient to guide MoE's model design, which motivates the development of new scaling laws tailored to MoE with these new-added factors. Recent studies have investigated MoE scaling laws based on certain MoE-specific factors, including the granularity of activated experts (Krajewski et al., 2024) and the activated model size (Ludziejewski et al., 2025). Different from them, our scaling law is more comprehensive and quantitatively defined considering five factors. As a result, our scaling law provides a more accurate fit to the loss, as shown in Fig. 5.

3 Experimental Setup

We systematically analyze the five key factors of MoE that influence training dynamics: data size D, total model size N, activated model size N_a, number of activated experts G and ratio of shared experts in activated experts S. To isolate their individual effects, we conduct 450 controlled experiments divided into several groups, each group varying a single target factor while holding the others fixed. This setup enables a clear assessment of how each factor impacts the validation loss.

Formally, we define the number of shared experts as n_s, the number of routed experts as n_e, the number of activated routed experts as n_k, the head dimension as d_{head}, the hidden dimension as d_{hidden}, the expert dimension as d_{expert}, the number of heads as n_h and the number of layers as l. Based on these definitions, the following relationships hold:

$$G = n_k + n_s, \quad N_a \approx \left(4d_{\text{head}} \cdot n_h + 3Gd_{\text{expert}}\right) d_{\text{hidden}} \cdot l, \tag{2}$$

$$S = \frac{n_s}{G}, \quad N \approx \left(4d_{\text{head}} \cdot n_h + 3d_{\text{expert}}(SG + n_e)\right) d_{\text{hidden}} \cdot l. \tag{3}$$

An MoE layer consists of multiple experts and a router that assigns tokens, often using a Top-K routing strategy with an auxiliary balance loss to ensure expert utilization. Training typically adopts standard optimizers such as AdamW (Kingma & Ba, 2014) with parallelism techniques (data, model and expert parallelism) for scalability. We select the widely-used classical MoE structures with architectural details provided in Appendix B. All experiments employ the Warmup-Stable-Decay (WSD) learning rate scheduler (Hu et al., 2024). For studies involving different values of D, we reused the same warmup and stable phases across runs to avoid redundant computation and reduce resource usage. All models are trained on a subset of the Dolma V1.7 dataset (Soldaini et al., 2024).

To fit the correlations between validation loss and five key factors, we systematically conduct experiments within controlled ranges of language model pretraining, with total model size $N \in [133\text{M}, 3.4\text{B}]$ and training data sizes $D \in [10\text{B}, 50\text{B}]$ tokens. We additionally vary the activated model size $N_a \in [30\text{M}, 2.2\text{B}]$, the number of activated experts $G \in [1, 20]$ and the ratio of shared experts $S \in [0.0, 0.7]$. For validation, we further extend to larger model and data sizes (up to 9B total model size and 100B trained tokens) and different MoE settings (up to 256 experts, 20 activated experts and 70% ratio of shared experts), successfully verifying the effectiveness and generalization ability of our scaling laws. The complete experimental settings are reported in Appendix L.

4 Our Scaling Laws for MoE

MoE has gradually emerged as a primary solution for the continuous scaling of model sizes and efficient deployment of LLMs. The core factors of MoE models exhibit higher complexity and strong inter-factor coupling compared to dense models and such inherent complexity renders the classical Chinchilla (Hoffmann et al., 2022) and OpenAI (Kaplan et al., 2020) scaling laws insufficient to guide the design of MoE architectures.

We aim to build a comprehensive and accurate MoE scaling law. In the following, we sequentially elaborate on the marginal effects of each core factor on MoE model performance via controlled-factor experiments, encompassing the total model size (N), data size (D), activated model size (N_a), number of activated experts (G) and the ratio of shared experts in activated experts (S). Building upon these analyses, we further derive the methodology underlying our joint MoE scaling law.

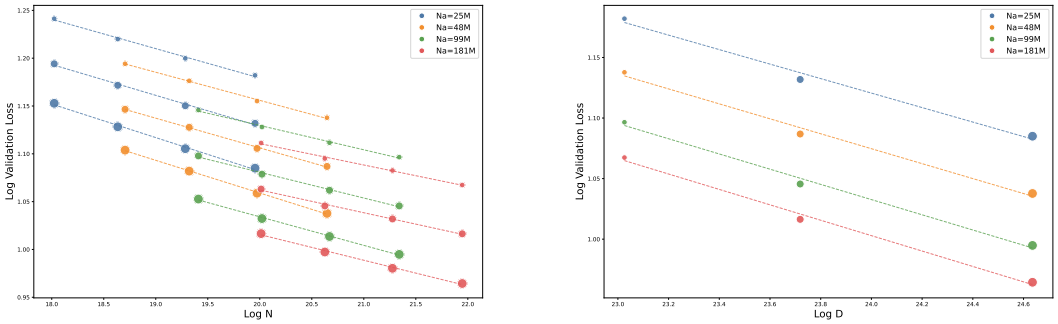

(a) Loss vs. N. (b) Loss vs. D.

Figure 1: Marginal effects of validation loss with respect to N and D under the logarithmic coordinate system. Data point sizes are directly proportional to D.

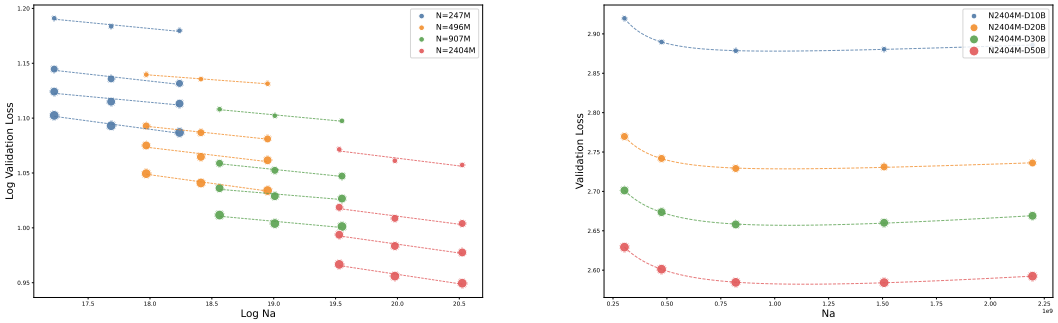

(a) Loss vs. N_a at small N_a/N ratios. (b) Loss vs. N_a across the entire N_a/N.

Figure 2: Marginal effects of validation loss with N_a. (a) illustrates the power-law-like marginal relationship between loss and N_a under smaller N_a/N. (b) indicates that loss oscillates and increases as N_a/N becomes increasingly large. Data point sizes are proportional to D.

4.1 The Basic MoE Scaling Law's Form with N and D

Total model size N and data size D constitute two primary factors influencing the performance of LLMs. Leveraging the scaling laws of dense models as a foundation, we examine whether N and D in MoE still conform to a power-law relationship. As illustrated in Figure 1, a distinct power-law relationship is observed between validation loss, total model size N and data size D.

Specifically, we increase N with G, S, D and N_a unchanged. By performing logarithmic transformations on both the validation loss and N, a linear relationship is observed across different ranges of model sizes—this confirms a significant power-law relationship between the loss and N. Similarly, a significant power-law relationship also exists between the loss and D. Furthermore, in Figure 1, we find that experimental groups with the same model size but varying data sizes exhibit a translation along the y-axis, which implies that N and D are mutually independent. From these observations, we conclude that the loss for MoE with respect to the total model size N and data size D is as:

$$L(N, D) = \frac{a}{N^{\alpha}} + \frac{b}{D^{\beta}} + \epsilon, \tag{4}$$

which has the same form of the Chinchilla scaling law (Hoffmann et al., 2022). The specific fitting results of Eq. 4 are provided in Appendix C.2.

4.2 Impact of Activated Model Size N_a

Activated model size N_a is a critical factor specific to MoE architectures that governs the balance between the model performance and efficiency. To gain deeper insights into the scaling law with

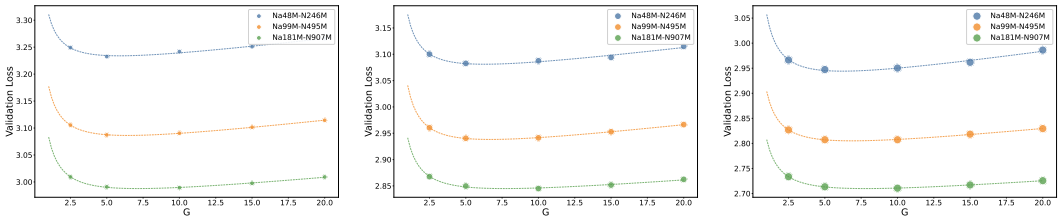

(a) Loss vs. G with 10B data size. (b) Loss vs. G with 20B data size. (c) Loss vs. G with 50B data size.

Figure 3: Marginal effects of validation loss with respect to G. (a), (b) and (c) illustrate the marginal relationship between loss and G under different D and N. Data point sizes are proportional to D.

N_a as an independent factor, we conducted multiple controlled experiments where N_a was the only varying factor. The formula followed by the controlled variable of N_a is detailed in Appendix H..

In Figure 2, the scaling of activated parameters N_a is achieved by increasing the expert dimension, while the total model size N is maintained constant through a corresponding reduction in the number of routed experts. When the ratio of N_a to N is small, a power-law-like relationship is exhibited between N_a and validation loss. However, as this ratio increases, the validation loss demonstrates a tendency to rise gradually, leading to an overall distribution that resembles a hook-like function, which is formalized as follows:

$$L(N_a) = \frac{c}{N_a^{\gamma}} + hN_a + \iota. \tag{5}$$

Next, we proceed to integrate the relationship involving N_a with those of data size D and total model size N. We performed hyperparameter fitting under different configurations of D and N, with the results presented in Figure 8. We observe that ι exhibits a negative correlation with both D and N, following a power-law distribution. In contrast, c and γ exhibit oscillations with variations in N and D, indicating that they bear no systematic relationship to N and D. Furthermore, h is negatively correlated with N, exhibiting an inversely proportional relationship, while showing no dependence on D. Therefore, the joint scaling law of N, D and N_a is concluded as follows:

$$L(N, D, N_a) = \frac{c}{N_a^{\gamma}} + h\frac{N_a}{N} + \iota L(N, D). \tag{6}$$

$L(N, D)$ denotes the basic scaling law sharing the same form in Eq. 4. Notably, our fitting results reveal that $\gamma \approx \alpha$. Hence, the final scaling law that governs $L(N, D, N_a)$ is formalized as follows:

$$L(N, D, N_a) = \frac{a}{N^{\alpha}} + \frac{b}{D^{\beta}} + \frac{c}{N_a^{\alpha}} + h\frac{N_a}{N} + \epsilon. \tag{7}$$

We explored alternative relationship forms of $L(N_a)$, performed relevant comparative experiments and derivations and ultimately established the aforementioned formulas describing the scaling law of N, D and N_a. Eq. 7 implies that N_a has an optimal value, which seems to be contrary to the prevalent assumption that "a larger N_a yields lower loss". It is because that when N_a/N exceeds a specific threshold with other factors (e.g., N and G) remains unchanged, the expert size increases progressively while the number of experts decreases. It induces gradual structural distortion in the MoE architecture, which in turn disrupt the advantage of MoE's combinational activation and thus degrades the performance. We have also validated that Eq. 7 can accurately predict the loss for models with larger model sizes. More discussions and detailed parameter fitting procedures are given in Appendix C.3 and F.

4.3 Impact of the Number of Activated Experts G

G constitutes another critical factor, defined as the number of activated experts (including activated shared and routed experts). It reflects the granularity of expert partitioning in MoE architectures. To investigate the scaling law with G as the independent factor, a series of controlled experiments were conducted with other factors constant, shown in Figure 3 and Figure 11. With the increase in G, the validation loss exhibits a trend of first decreasing and then increasing. It is hypothesized that the impact of G better conforms to a hook function relationship, expressed as follows:

$$L(G) = eG + \frac{f}{G} + \tau. \tag{8}$$

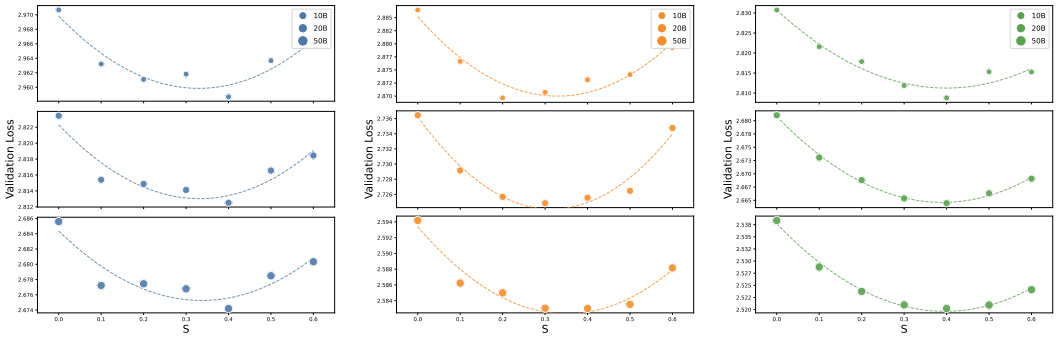

(a) Loss vs. S: Na240M-N1.2B. (b) Loss vs. S: Na476M-N2.4B. (c) Loss vs. S: Na793M-N4B.

Figure 4: Marginal effects of validation loss with respect to S. (a), (b) and (c) respectively illustrate the marginal relations between loss and S under different N, D settings. For small N and D, the trend of S is taking shape but is also easily affected by noise. As they increase, the scaling law of S gradually becomes significant and robust. More details are in Appendix C.5.

It is noteworthy that the possible G's exponent term approaches 1. Therefore, based on the fitting results and the Occam's Razor principle (Blumer et al., 1987), the exponent term of G is omitted.

4.4 The Joint MoE Scaling Law of N, D, N_a and G

Based on the above conclusions in Eq. 7 and 8, we explore the variation patterns of the fitted hyperparameters $a, \alpha, b, \beta, c, h, \epsilon$ under different values of G. We observe that a, c and h exhibit the hook-function trend with variations in G, whereas other hyperparameters are largely unaffected by G and display no discernible pattern in Figure 10. Hence, we can express them as $a = e_1 G + \frac{f_1}{G} + \tau_1$, $c = e_2 G + \frac{f_2}{G} + \tau_2$ and $h = e_3 G + \frac{f_3}{G} + \tau_3$. Furthermore, after re-parameterizing them, we notably found that (e_1, f_1), (e_2, f_2) and (e_3, f_3) exhibit a proportional correlation and $\tau_3 \approx 0$. Therefore, the scaling law for $L(N, D, N_a, G)$ is presented as follows:

$$L(N, D, N_a, G) = (eG + \frac{f}{G}) * (\frac{1}{N^\alpha} + \frac{k}{N_a^\alpha} + h\frac{N_a}{N}) + \frac{a}{N^\alpha} + \frac{b}{D^\beta} + \frac{c}{N_a^\alpha} + \epsilon. \tag{9}$$

Here, $\frac{a}{N^\alpha} + \frac{b}{D^\beta} + \epsilon$ denotes the basic Chinchilla-like scaling law part from Eq. 4. Considering that N_a and N exhibit a similar mechanism of action on the loss to a certain extent, we also have a power-law term $\frac{c}{N_a^\alpha}$ for N_a. The right terms $\frac{a}{N^\alpha} + \frac{b}{D^\beta} + \frac{c}{N_a^\alpha} + \epsilon$ could be viewed to characterize the scaling law with respect to (activated/total) model size and data size. For the left term, $eG + \frac{f}{G}$ denotes the effect of G (related to MoE expert structure) on loss from Eq. 8 and such effect is scaled by the model size factors ($\frac{1}{N^\alpha} + \frac{k}{N_a^\alpha} + h\frac{N_a}{N}$, which is non-monotonic for N_a introduced in Eq. 7). The detailed analysis of hyperparameters and fitting results of Eq. 9 are provided in Appendix C.4.

4.5 Extended Joint MoE Scaling Law with Shared Expert Ratio S

The shared experts have been verified to be essential in popular MoE architectures (Dai et al., 2024; Liu et al., 2025). We set the shared expert ratio S ($S = n_s/G$, where n_s represents the number of shared experts) as the sole varying factor to conduct experiments as presented in Figure 4. We find that MoE models with shared experts significantly outperform those without shared experts, verifying the necessity of shared expert isolation. As S increases, the loss first decreases and then increases, while it exerts a relatively minor impact on losses around the optimal point. Based on these observations, we adopt a quadratic function to capture the marginal effect of S on the loss.

$$L(S) = mS^2 + nS + \psi. \tag{10}$$

Final Joint MoE Scaling Law. We then incorporate S into Eq. 9 to build our final joint MoE scaling law with all five factors. Given that S exerts only a minor influence on loss in a wide range, we assume that S has negligible impact on the form and hyperparameters. Accordingly, we perform

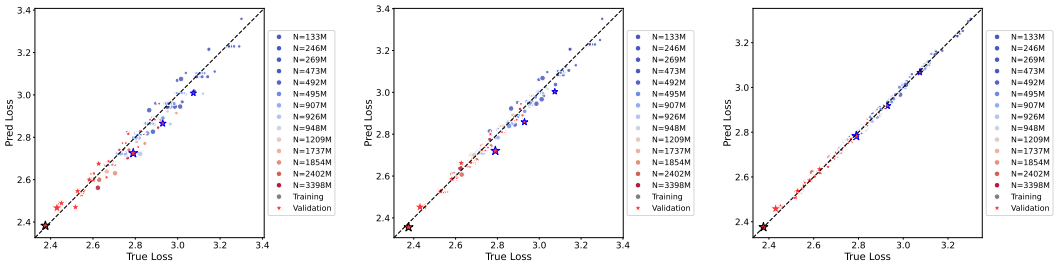

(a) Krajewski et al. (2024). (b) Abnar et al. (2025). (c) Ours.

Figure 5: Fitting results of existing and our joint scaling laws for MoE architectures. The average validation loss errors of (a), (b) and (c) are respectively 0.0193, 0.0170 and 0.0060. Star points are validation data with larger model sizes, larger data sizes and different MoE settings. Data point size is proportional to D. Detailed descriptions of compared scaling laws are provided in Appendix I.

hyperparameter fitting for Eq. 10 across diverse configurations of N, D, N_a and G and analyze the relationships between these fitted hyperparameters and factors. The results are presented in Figure 13 with key findings: (1) m and n are independent of D, indicating that D and S are mutually decoupled; (2) m increases with the growth of N and N_a, whereas n decreases with the growth of N and N_a. Notably, the extreme point of S remains unchanged with variations in N and N_a; (3) ψ exhibits an obvious power-law relationship with N, N_a and D; (4) As can be inferred from the definition of S in Eq. 3, S is already correlated with G, so its relationship with G will not be further considered. Considering the compatibility with Eq. 9, the form of $L(N, D, N_a, G, S)$ is expressed as: $(L(G) + L(S)) * \phi(N, N_a) + \frac{a}{N^\alpha} + \frac{b}{D^\beta} + \frac{c}{N_a^\alpha} + \epsilon$. Consequently, we propose our MoE scaling law comprehensively with N, D, N_a, G, S as follows:

$$L(N, D, N_a, G, S) = (eG + \frac{f}{G} + mS^2 + nS) * (\frac{1}{N^\alpha} + \frac{k}{N_a^\alpha} + h\frac{N_a}{N}) + \frac{a}{N^\alpha} + \frac{b}{D^\beta} + \frac{c}{N_a^\alpha} + \epsilon. \quad (11)$$

Note that the factors of S and G, which jointly characterize the MoE structure of activated experts, are included in the first term, while the other terms remain consistent with those in Eq. 9. Their impact on the loss is also regulated by the total model size N and the activated model size N_a. A detailed analysis of hyperparameters is presented in Appendix C.5.

Fitting Results. To determine the specific value of hyperparameters in Eq. 11, we implement all 450 experiments that encompass diverse configurations of N, D, N_a, G and S. The corresponding hyperparameter values are provided in Table 2 in Appendix C.1. Next, we evaluate the fitting performance of our MoE scaling law in Figure 5, where the satisfactory fitting performance demonstrates the advantage of our MoE scaling law compared to others. Notably, for the sake of fairness, during the comparison, the baseline MoE scaling laws were first re-fitted with hyperparameters using the same data points, followed by prediction. Moreover, we extend the experiments to larger MoE models (up to 9B total model size and 100B trained tokens) with different MoE structure settings (G ranges from 2 to 20 and S ranges from 0 to 0.7). The consistently accurate fitting results demonstrate that our scaling law maintains robust performance when applied to larger-scale MoE models with broad ranges of parameter selections.

5 Key Implications for MoE Architecture Design

In this section, we discuss the insightful findings deduced on the basis of our MoE scaling laws, which are anticipated to provide more effective guidance for the design of better MoE models.

5.1 Implication-1: Optimal Number of Activated Experts G

In light of Eq. 11, the optimal number of activated experts G can be expressed as follows:

$$G_{opt} = \sqrt{f/e}. \quad (12)$$

Eq. 12 demonstrates that the optimal G is independent of model size N, activated model size N_a and data size D, thereby corresponding to a fixed optimal value $G_{opt} \approx 6.78$. Moreover,

the theoretically derived optimal G exhibits strong alignment with the configurations employed by current mainstream MoE models, including DeepSeek-V3.1 (Liu et al., 2024), Kimi-K2 (Kimi et al., 2025) and Qwen3-235B-A22B (Qwen Team et al., 2025) (both $G = 8$ *or* 9). The detailed formula derivation is provided in Appendix D.

5.2 Implication-2: Optimal Ratio of shared experts S

Similarly, S is independent of other factors and also has an optimal value as follows:

$$S_{opt} = -n/2m. \tag{13}$$

Eq. 13 shows that the optimal $S \approx 0.31$ is also independent of other factors. As shown in Table 3, since S has minor impact on loss around the optimal point as stated in Section 4.5, the appropriate S values are approximately distributed in the range of $[0.13, 0.31]$ for the majority of popular MoE settings, with the loss deviation to the optimal setting's less than 0.001. In conclusion, our findings lead to the following recommendation: the shared expert constitutes an essential component. For the optimal total activated expert number $G = 7$, we could set 1 or 2 shared experts. Notably, this aligns with the architectural configurations observed in open-source canonical MoE models, corroborating the validity of our conclusions. More details and analyses are in Appendix E.

5.3 Implication-3: Optimal Activated Parameter Ratio N_a/N

Theoretical Analysis. From Eq. 11, it can be observed that there are two types of terms involving the activated model size N_a as a numerator or denominator. These two terms exert opposite effects on the loss of MoE models. Intuitively, this implies that there exists an optimal N_a given the configurations of other factors (e.g., the model size N). Given N, the $(\frac{N_a}{N})_{opt_t}$ that achieves the theoretically optimal loss is formalized as follows (Comprehensive derivation is in Appendix F):

$$\left(\frac{N_a}{N}\right)_{opt_t} = \left(\frac{\alpha \cdot \left[k \cdot \left(eG + \frac{f}{G} + mS^2 + nS\right) + c\right]}{hN^{\alpha} \cdot \left(eG + \frac{f}{G} + mS^2 + nS\right)}\right)^{\frac{1}{\alpha+1}} = \left(\frac{\alpha \cdot [k \cdot const + c]}{hN^{\alpha} \cdot const}\right)^{\frac{1}{\alpha+1}}. \tag{14}$$

According to our Implications #1 and #2, G and S have optimal values and thus $eG + \frac{f}{G} + mS^2 + nS$ can be represented as a constant term $const$ under the optimal setting. Eq. 14 indicates that the optimal $(\frac{N_a}{N})_{opt_t}$ decreases as the model size N increases. It verifies that with the increasing total model sizes, the optimal MoE architecture will be sparser with smaller N_a, which is consistent with the current trend of MoE models (Kimi et al., 2025; OpenAI et al., 2025). For instance, for N from 30B (Qwen3-30B-A3B (Qwen Team et al., 2025)) to 671B (Deepseek-V3.1 (Liu et al., 2024)), the theoretically optimal ratio satisfies $(\frac{N_a}{N})_{opt_t}$ range from 40.0% to 22.0%.

Practical Efficiency-aware Analysis. However, the theoretically optimal sparsity degree of MoE $\frac{N_a}{N}$ calculated in Eq. 14 cannot be directly used to guide the real-world MoE architecture design, as the efficiency of LLMs is also an essential factor. Specifically, when N_a gradually increases toward its optimal value, the performance gains become increasingly marginal, while the associated costs rise steadily. Therefore, it is necessary to explore more practical efficiency-aware optimal $(\frac{N_a}{N})_{opt_e}$ under the consideration of the balance between performance gain and efficiency cost.

Specifically, we define the loss gain threshold as ΔLoss for the step size of ΔN_a set as $0.01N$. As N_a is incrementally scaled for each step size, the marginal gain of loss reduction will ultimately fall below the loss gain threshold ΔLoss, where we suppose the model reaches the practical efficiency-aware optimal $(\frac{N_a}{N})_{opt_e}$. Comprehensive derivation and pseudo code are in Appendix F. Hence, for a given model size N, our MoE scaling law yields a practically applicable range for N_a, spanning the interval from the practical efficiency-aware optimal point to the theoretical optimal point, i.e., $N_a \in [(\frac{N_a}{N})_{opt_e}, (\frac{N_a}{N})_{opt_t}]$. To substantiate the validity of our conclusions, we conducted an analysis on the configurations of mainstream industrial MoE models, with detailed specifications in Table 4. It shows that the activated model sizes of most mainstream MoE models are within our recommended range above. Note that some recent MoE models (e.g., Kimi-K2 (Kimi et al., 2025) and gpt-oss-120b (OpenAI et al., 2025)) employ a more aggressive sparser architecture with $\frac{N_a}{N} \leq 4\%$, primarily aiming to reduce the training/inference costs in practice with larger total model sizes.

6 Related Work

6.1 MoE Architecture

In the field of language models, the MoE model enables experts to learn different knowledge and combine their outputs (Abdin et al., 2024; Team et al., 2025; Zeng et al., 2025; Lieber et al., 2024). Shazeer et al. (2017) expanded upon this with the Sparsely-Gated Mixture-of-Experts (SMoE) layer and Top-K routing, which selects a fixed number of experts for each token. This was further developed by Gshard (Lepikhin et al., 2020) and SwitchTransformer (Fedus et al., 2022) by integrating MoE into Transformer feedforward layers with Top-1 and Top-2 routing. More recently, Dai et al. (2024) proposed modifying the MoE layer by subdividing experts into smaller experts and adding shared experts into the architecture. These advancements continue to enhance the efficiency and flexibility of MoE. At the same time, there is a trend toward scaling MoE to larger model sizes and to a greater number of experts, as shown in recent works such as K2 (Kimi et al., 2025), DeepSeek-V3 (Liu et al., 2024) and Mixture of a Million Experts (He, 2024). In parallel, several studies have investigated alternative routing strategies and expert designs, including heterogeneous experts in HMoE (Wang et al., 2024a), autonomous expert activation in AoE (Lv et al., 2025) and probabilistic Top-P routing (Zhou et al., 2022). In this work, when analyzing scaling laws, we adopt the classical Top-K routing strategy as our main setting.

6.2 Scaling Laws of LLMs

Scaling laws for LLMs describe how model performance depends on factors such as model size and training data. In dense Transformers, Kaplan et al. (2020) first studied scaling laws and showed that the final model perplexity follows a power-law relationship with both model size and data size. Building on this, Hoffmann et al. (2022) extended the analysis by incorporating variable cosine cycle lengths and proposed a revised scaling formulation. Scaling behavior has also been examined in alternative architectures and training regimes, particularly in MoE models. Clark et al. (2022) investigated MoE scaling laws under a fixed dataset, focusing on the impact of model size and the number of experts. Krajewski et al. (2024) studied how scaling changes with different levels of expert granularity in MoE architectures. Abnar et al. (2025) analyzed scaling laws with respect to total model size N, dataset size D and the fraction of inactive experts, while Ludziejewski et al. (2025) examined the joint effects of multiple factors, including the activated model size N_a, dataset size D. The comparison between these scaling laws and ours is in Table 5.

Beyond architectures, Step Law (Li et al., 2025a) and relevant studies (Shuai et al., 2024; Zhang et al., 2024; McCandlish et al., 2018) provide principles for learning rate, weight decay and batch size, while Farseer (Li et al., 2025b) refines loss scaling for accurate extrapolation. Other works include parallel scaling (Chen et al., 2025) for improving compute efficiency and SynthLLM (Qin et al., 2025) for analyzing the scalability of synthetic data. More recently, Sun et al. (2025) proposed a joint scaling law for floating point quantization training, highlighting the influence of exponent and mantissa bits, the effect of critical data size and the optimal precision range for efficient LLM training. Overall, these works extend scaling laws across optimizers, architectures and data, providing guidance for LLM design and training. Nevertheless, the community is urgent to build a more comprehensive MoE scaling law.

7 Conclusion and Future Work

In this work, we propose a more accurate joint MoE scaling law that considers more comprehensive factors, including total model size N, data size D, activated model size N_a, the number of activated experts G and the ratio of shared experts in activated experts S. Based on the joint MoE scaling law, we further derive the optimal value expressions for essential MoE-specific factors of G, S and N_a/N and identify several insightful implications, which can facilitate future MoE model design and training. In the future, we will further validate our scaling law under larger scales and novel MoE architectures. Currently, our investigations have primarily centered on factors pertaining to the MoE blocks. It would be worthwhile to extend this scope to encompass both the factors and structural configurations associated with other LLM blocks, such as the attention layers.

Reproducibility Statement

To ensure the reproducibility of our results, we have taken the following measures: (1) **Datasets**. In Section 3, we specify the dataset (Dolma V1.7 dataset) used in the experiments and provide its source attribution. (2) **Code**. All experiments in our scaling law research were trained using open-source frameworks (Megatron and Torchtitan), ensuring high reproducibility. Details are provided in the supplementary materials. (3) **Experimental Details**. The basic experimental settings are described in Section 3, with specific hyperparameter configurations provided in Appendix B and detailed experimental specifications in Appendix L. (4) **Proof Details**. The derivation process of our joint MoE scaling law is elaborated in detail in Section 4 and Appendix C. Meanwhile, the derivation of the key implications involved is thoroughly explained in Section 5, as well as in Appendices D, E, F and G.

References

Marah Abdin, Jyoti Aneja, Harkirat Behl, Sébastien Bubeck, Ronen Eldan, Suriya Gunasekar, Michael Harrison, Russell J Hewett, Mojan Javaheripi, Piero Kauffmann, et al. Phi-4 technical report. *arXiv preprint arXiv:2412.08905*, 2024.

Samira Abnar, Harshay Shah, Dan Busbridge, Alaaeldin Mohamed Elnouby Ali, Josh Susskind, and Vimal Thilak. Parameters vs flops: Scaling laws for optimal sparsity for mixture-of-experts language models. *arXiv preprint arXiv:2501.12370*, 2025.

Anselm Blumer, Andrzej Ehrenfeucht, David Haussler, and Manfred K Warmuth. Occam's razor. *Information processing letters*, 24(6):377–380, 1987.

Mouxiang Chen, Binyuan Hui, Zeyu Cui, Jiaxi Yang, Dayiheng Liu, Jianling Sun, Junyang Lin, and Zhongxin Liu. Parallel scaling law for language models. *arXiv preprint arXiv:2505.10475*, 2025.

Aidan Clark, Diego de Las Casas, Aurelia Guy, Arthur Mensch, Michela Paganini, Jordan Hoffmann, Bogdan Damoc, Blake Hechtman, Trevor Cai, Sebastian Borgeaud, et al. Unified scaling laws for routed language models. In *International conference on machine learning*, pp. 4057–4086. PMLR, 2022.

Damai Dai, Chengqi Deng, Chenggang Zhao, RX Xu, Huazuo Gao, Deli Chen, Jiashi Li, Wangding Zeng, Xingkai Yu, Yu Wu, et al. Deepseekmoe: Towards ultimate expert specialization in mixture-of-experts language models. *arXiv preprint arXiv:2401.06066*, 2024.

Abhimanyu Dubey, Abhinav Jauhri, Abhinav Pandey, Abhishek Kadian, Ahmad Al-Dahle, Aiesha Letman, Akhil Mathur, Alan Schelten, Amy Yang, Angela Fan, et al. The llama 3 herd of models. *arXiv e-prints*, pp. arXiv–2407, 2024.

William Fedus, Barret Zoph, and Noam Shazeer. Switch transformers: Scaling to trillion parameter models with simple and efficient sparsity. *Journal of Machine Learning Research*, 23(120):1–39, 2022.

Xu Owen He. Mixture of a million experts. *arXiv preprint arXiv:2407.04153*, 2024.

Jordan Hoffmann, Sebastian Borgeaud, Arthur Mensch, Elena Buchatskaya, Trevor Cai, Eliza Rutherford, Diego de Las Casas, Lisa Anne Hendricks, Johannes Welbl, Aidan Clark, et al. Training compute-optimal large language models. *arXiv preprint arXiv:2203.15556*, 2022.

Shengding Hu, Yuge Tu, Xu Han, Chaoqun He, Ganqu Cui, Xiang Long, Zhi Zheng, Yewei Fang, Yuxiang Huang, Weilin Zhao, et al. Minicpm: Unveiling the potential of small language models with scalable training strategies. *arXiv preprint arXiv:2404.06395*, 2024.

Albert Q Jiang, Alexandre Sablayrolles, Antoine Roux, Arthur Mensch, Blanche Savary, Chris Bamford, Devendra Singh Chaplot, Diego de las Casas, Emma Bou Hanna, Florian Bressand, et al. Mixtral of experts. *arXiv preprint arXiv:2401.04088*, 2024.

Jared Kaplan, Sam McCandlish, Tom Henighan, Tom B Brown, Benjamin Chess, Rewon Child, Scott Gray, Alec Radford, Jeffrey Wu, and Dario Amodei. Scaling laws for neural language models. *arXiv preprint arXiv:2001.08361*, 2020.

Team Kimi, Yifan Bai, Yiping Bao, Guanduo Chen, Jiahao Chen, Ningxin Chen, Ruijue Chen, Yanru Chen, Yuankun Chen, Yutian Chen, et al. Kimi k2: Open agentic intelligence. *arXiv preprint arXiv:2507.20534*, 2025.

Diederik P Kingma and Jimmy Ba. Adam: A method for stochastic optimization. *arXiv preprint arXiv:1412.6980*, 2014.

Jakub Krajewski, Jan Ludziejewski, Kamil Adamczewski, Maciej Pióro, Michał Krutul, Szymon Antoniak, Kamil Ciebiera, Krystian Król, Tomasz Odrzygóźdź, Piotr Sankowski, et al. Scaling laws for fine-grained mixture of experts. *arXiv preprint arXiv:2402.07871*, 2024.

Dmitry Lepikhin, HyoukJoong Lee, Yuanzhong Xu, Dehao Chen, Orhan Firat, Yanping Huang, Maxim Krikun, Noam Shazeer, and Zhifeng Chen. Gshard: Scaling giant models with conditional computation and automatic sharding. *arXiv preprint arXiv:2006.16668*, 2020.

Houyi Li, Wenzhen Zheng, Jingcheng Hu, Qiufeng Wang, Hanshan Zhang, Zili Wang, Shijie Xuyang, Yuantao Fan, Shuigeng Zhou, Xiangyu Zhang, et al. Predictable scale: Part i–optimal hyperparameter scaling law in large language model pretraining. *arXiv e-prints*, pp. arXiv–2503, 2025a.

Houyi Li, Wenzhen Zheng, Qiufeng Wang, Zhenyu Ding, Haoying Wang, Zili Wang, Shijie Xuyang, Ning Ding, Shuigeng Zhou, Xiangyu Zhang, et al. Farseer: A refined scaling law in large language models. *arXiv preprint arXiv:2506.10972*, 2025b.

Wanchao Liang, Tianyu Liu, Less Wright, Will Constable, Andrew Gu, Chien-Chin Huang, Iris Zhang, Wei Feng, Howard Huang, Junjie Wang, et al. Torchtitan: One-stop pytorch native solution for production ready llm pre-training. *arXiv preprint arXiv:2410.06511*, 2024.

Opher Lieber, Barak Lenz, Hofit Bata, Gal Cohen, Jhonathan Osin, Itay Dalmedigos, Erez Safahi, Shaked Meirom, Yonatan Belinkov, Shai Shalev-Shwartz, et al. Jamba: A hybrid transformer-mamba language model. *arXiv preprint arXiv:2403.19887*, 2024.

Aixin Liu, Bei Feng, Bing Xue, Bingxuan Wang, Bochao Wu, Chengda Lu, Chenggang Zhao, Chengqi Deng, Chenyu Zhang, Chong Ruan, et al. Deepseek-v3 technical report. *arXiv preprint arXiv:2412.19437*, 2024.

Ao Liu, Botong Zhou, Can Xu, Chayse Zhou, ChenChen Zhang, Chengcheng Xu, Chenhao Wang, Decheng Wu, Dengpeng Wu, et al. Hunyuan-turbos: Advancing large language models through mamba-transformer synergy and adaptive chain-of-thought. *arXiv preprint arXiv:2505.15431*, 2025.

Jan Ludziejewski, Maciej Pióro, Jakub Krajewski, Maciej Stefaniak, Michał Krutul, Jan Małaśnicki, Marek Cygan, Piotr Sankowski, Kamil Adamczewski, Piotr Miłoś, et al. Joint moe scaling laws: Mixture of experts can be memory efficient. *arXiv preprint arXiv:2502.05172*, 2025.

Ang Lv, Ruobing Xie, Yining Qian, Songhao Wu, Xingwu Sun, Zhanhui Kang, Di Wang, and Rui Yan. Autonomy-of-experts models. *arXiv preprint arXiv:2501.13074*, 2025.

Sam McCandlish, Jared Kaplan, Dario Amodei, and OpenAI Dota Team. An empirical model of large-batch training. *arXiv preprint arXiv:1812.06162*, 2018.

Sandhini OpenAI, Agarwal, Lama Ahmad, Jason Ai, Sam Altman, Andy Applebaum, Edwin Arbus, Rahul K Arora, Yu Bai, Bowen Baker, Haiming Bao, et al. gpt-oss-120b & gpt-oss-20b model card. *arXiv preprint arXiv:2508.10925*, 2025.

Zeyu Qin, Qingxiu Dong, Xingxing Zhang, Li Dong, Xiaolong Huang, Ziyi Yang, Mahmoud Khademi, Dongdong Zhang, Hany Hassan Awadalla, Yi R Fung, et al. Scaling laws of synthetic data for language models. *arXiv preprint arXiv:2503.19551*, 2025.

An Qwen Team, Yang, Anfeng Li, Baosong Yang, Beichen Zhang, Binyuan Hui, Bo Zheng, Bowen Yu, Chang Gao, Chengen Huang, Chenxu Lv, et al. Qwen3 technical report. *arXiv preprint arXiv:2505.09388*, 2025.

Noam Shazeer, Azalia Mirhoseini, Krzysztof Maziarz, Andy Davis, Quoc Le, Geoffrey Hinton, and Jeff Dean. Outrageously large neural networks: The sparsely-gated mixture-of-experts layer. *arXiv preprint arXiv:1701.06538*, 2017.

Mohammad Shoeybi, Mostofa Patwary, Raul Puri, Patrick LeGresley, Jared Casper, and Bryan Catanzaro. Megatron-lm: Training multi-billion parameter language models using model parallelism. *arXiv preprint arXiv:1909.08053*, 2019.

Xian Shuai, Yiding Wang, Yimeng Wu, Xin Jiang, and Xiaozhe Ren. Scaling law for language models training considering batch size. *arXiv preprint arXiv:2412.01505*, 2024.

Luca Soldaini, Rodney Kinney, Akshita Bhagia, Dustin Schwenk, David Atkinson, Russell Authur, Ben Bogin, Khyathi Chandu, Jennifer Dumas, Yanai Elazar, et al. Dolma: An open corpus of three trillion tokens for language model pretraining research. *arXiv preprint arXiv:2402.00159*, 2024.

Xingwu Sun, Yanfeng Chen, Yiqing Huang, Ruobing Xie, Jiaqi Zhu, Kai Zhang, Shuaipeng Li, Zhen Yang, Jonny Han, Xiaobo Shu, et al. Hunyuan-large: An open-source moe model with 52 billion activated parameters by tencent. *arXiv preprint arXiv:2411.02265*, 2024.

Xingwu Sun, Shuaipeng Li, Ruobing Xie, Weidong Han, Kan Wu, Zhen Yang, Yixing Li, An Wang, Shuai Li, Jinbao Xue, et al. Scaling laws for floating point quantization training. In *Proceeding of ICML*, 2025.

Meituan LongCat Team, Bei Li, Bingye Lei, Bo Wang, Bolin Rong, Chao Wang, Chao Zhang, Chen Gao, Chen Zhang, Cheng Sun, et al. Longcat-flash technical report. *arXiv preprint arXiv:2509.01322*, 2025.

An Wang, Xingwu Sun, Ruobing Xie, Shuaipeng Li, Jiaqi Zhu, Zhen Yang, Pinxue Zhao, JN Han, Zhanhui Kang, Di Wang, et al. Hmoe: Heterogeneous mixture of experts for language modeling. *arXiv preprint arXiv:2408.10681*, 2024a.

Siqi Wang, Zhengyu Chen, Bei Li, Keqing He, Min Zhang, and Jingang Wang. Scaling laws across model architectures: A comparative analysis of dense and moe models in large language models. *arXiv preprint arXiv:2410.05661*, 2024b.

Aohan Zeng, Xin Lv, Qinkai Zheng, Zhenyu Hou, Bin Chen, Chengxing Xie, Cunxiang Wang, Da Yin, Hao Zeng, Jiajie Zhang, et al. Glm-4.5: Agentic, reasoning, and coding (arc) foundation models. *arXiv preprint arXiv:2508.06471*, 2025.

Hanlin Zhang, Depen Morwani, Nikhil Vyas, Jingfeng Wu, Difan Zou, Udaya Ghai, Dean Foster, and Sham Kakade. How does critical batch size scale in pre-training? *arXiv preprint arXiv:2410.21676*, 2024.

Yanqi Zhou, Tao Lei, Hanxiao Liu, Nan Du, Yanping Huang, Vincent Zhao, Andrew M Dai, Quoc V Le, James Laudon, et al. Mixture-of-experts with expert choice routing. *Advances in Neural Information Processing Systems*, 35:7103–7114, 2022.

A THE USE OF LARGE LANGUAGE MODELS (LLMS)

In this paper, we leveraged LLMs to support and refine the writing. Specifically, LLMs were used for grammar and spelling correction, as well as polishing linguistic expressions to enhance clarity and readability. All other core components of the work, including the development of ideas, design and execution of experiments and derivation of formulas, were completed manually by ourselves.

B HYPERPARAMETER DETAILS

We report serveral typical hyper-parameters used for training our MoE models in Table 1. The models vary in layers, hidden size and expert size across different scales, while the optimizer and learning rate settings are consistent. All models are trained with AdamW and cosine learning rate decay, using a sequence length of 2048 and a batch size of 2M tokens. The detailed hyper-parameters of our MoE models are given as follows. In all of our experiments, the parameters considered do not include those from the embedding layer. For all experimental settings, refer to Appendix L.

Table 1: Typical model hyper-parameters for different sizes.

Total model size Activated model size	247M 48M	496M 99M	907M 181M	2.40B 476M	3.96B 793M
# Layers	12	12	12	20	24
# Routed experts	32	32	32	32	32
# Activated routed experts	4	4	4	4	4
# Shared experts	1	1	1	1	1
# Attention heads	8	12	16	20	24
Hidden size	512	768	1024	1280	1536
Expert size	384	512	704	896	1024
Attention head size	64	64	64	64	64
Optimizer	AdamW				
Adam (β_1, β_2)	(0.9, 0.95)				
Adam ϵ	1×10^{-8}				
Weight decay	0.1				
Clip grad norm	1.0				
Max lr	3.0×10^{-4}				
Min lr	0				
Lr decay	Cosine				
Decay rate	10%				
Sequence length	2048				
Batch size (# tokens)	2M				
Warmup steps	500				
Normalization	RMSNorm				
Vocabulary size	128256				
Positional encoding	ROPE				

C FITTING DETAILS OF OUR MOE SCALING LAWS

Our MoE scaling law precisely characterizes the effects of three critical dimensions—parameters, data sizes and model architectures—on scaling patterns. Specifically, the term $L(G, S) \cdot \phi(N_a, N)$ quantifies the architectural impact on loss, while explicitly revealing its regulation by parameter scale. The formulation $\rho(N, D, N_a) = \frac{a}{N^\alpha} + \frac{b}{D^\beta} + \frac{c}{N_a^\alpha} + \epsilon$ delineates how parameters and data size influence the MoE loss. By integrating all core factors that govern MoE architectural performance into a joint scaling law, our proposed MoE scaling law achieves an elegant integration. This theoretical construct carries substantial significance for informing the design of MoE model architectures. Further details regarding the fitting process of our MoE scaling laws are elaborated below.

C.1 Numberical Fits of Our Joint MoE Scaling Law

Our joint MoE scaling law is formalized as:

$$L(N, D, N_a, G, S) = (eG + \frac{f}{G} + mS^2 + nS) * (\frac{1}{N^\alpha} + \frac{k}{N_a^\alpha} + h\frac{N_a}{N}) + \frac{a}{N^\alpha} + \frac{b}{D^\beta} + \frac{c}{N_a^\alpha} + \epsilon, \quad (15)$$

where the detailed fitted constants and values are presented below, based on 450 experiments across different model settings. Of these, 268 were used for fitting, 91 for validation, and 90 small-size experiments to observe the marginal effect of G.

Table 2: Fitted constants and their values in Eq. 15.

Constant	Value
e	0.1577
f	7.2446
m	5.1395
n	-3.2363
k	0.0013
h	0.0450
a	38.0510
α	0.2383
b	27129.0488
β	0.4694
c	31.0958
ϵ	1.8182

C.2 Fitting Results of the Scaling Law for $L(N, D)$

Figure 6 presents the fitting performance of the $L(N, D)$ Eq. 4 in fitting the loss of MoE architectures, where only total model size N and data size D are considered. It can be observed that $L(N, D)$ only provides a coarse-grained fit to our experimental data points, with suboptimal specific fitting performance. This indicates that additional factors within the MoE architecture need to be taken into account.

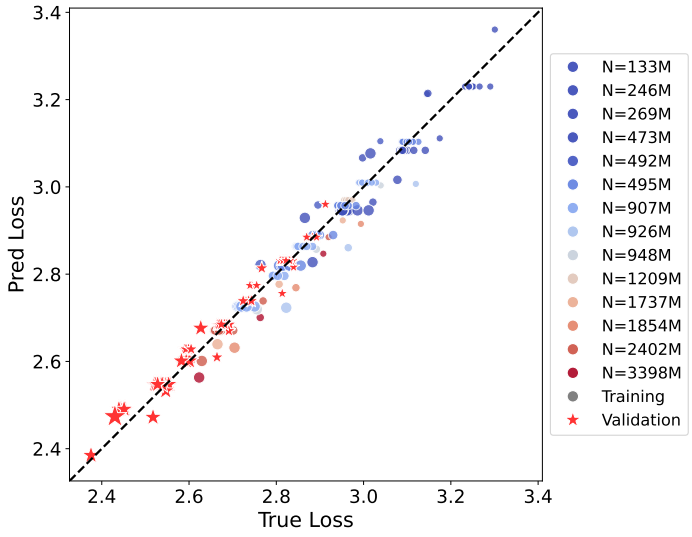

Figure 6: Fitting results of the scaling law of $L(N, D)$. Average validation loss error: 0.0179.

C.3 Fitting Results of the Scaling Law for $L(N, D, N_a)$

Figure 7 demonstrates the fitting performance of the scaling law $L(N, D, N_a)$ Eq. 7 on the loss of MoE models, where N_a is incorporated into the law. This result indicates that N_a constitutes a critical factor influencing the MoE scaling law and the inclusion of N_a in the joint scaling law yields a substantial improvement in fitting performance compared to the original scaling law $L(N, D)$.

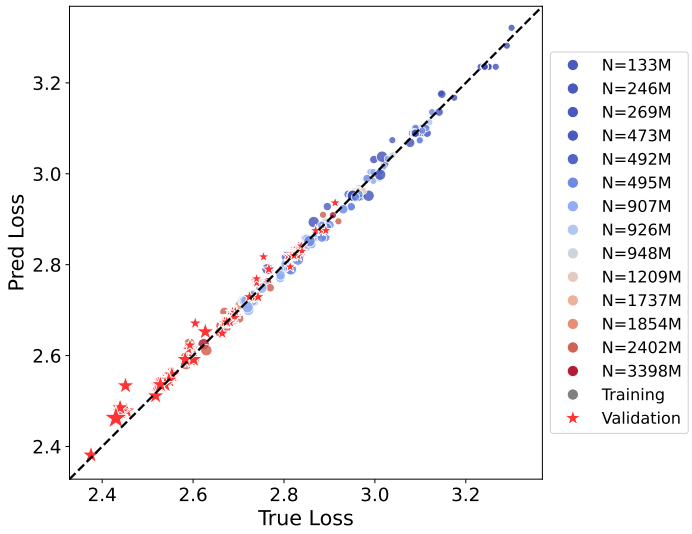

Figure 7: Fitting results of the scaling law of $L(N, D, N_a)$. Average validation loss error: 0.0124.

In the following, we elaborate on the process of incorporating the factor N_a into the scaling law $L(N, D, N_a)$ Eq. 7. Specifically, we first designed and conducted a series of controlled experiments on N_a following Eq. 35. Subsequently, hyperparameter fitting was performed across diverse configurations of D and N, with the associated results presented in Figure 8.

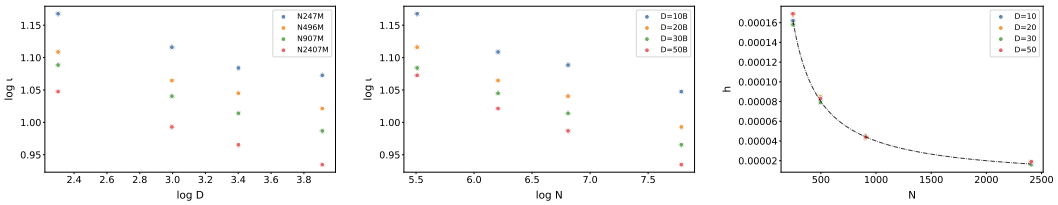

Figure 8: The correlations between ι, h in Eq. 5 and N, D. ι and h can be viewed as functions of N or D.

It can be observed that ι exhibits a linear relationship with N and D after logarithmic transformation, indicating a power-law relationship between ι and N as well as D. The parameter h shows an inverse proportional relationship with N across different data volumes D. Other factors c and γ fluctuate with changes in N and D without displaying obvious correlations and thus are considered independent of N and D. It is noteworthy that the hyperparameter fitting results indicate the fitted value of the exponent term for N_a in the term $h\frac{N_a}{N}$ approaches 1. Therefore, it is reasonable to conclude that N_a in the term $h\frac{N_a}{N}$ does not have an exponent.

C.4 Fitting Results of the Scaling Law for $L(N, D, N_a, G)$

Figure 9 illustrates the fitting performance of the scaling law $L(N, D, N_a, G)$ Eq. 9 on the loss of MoE architectures, where the granularity G is incorporated. As stated in Section 4.3, G characterizes

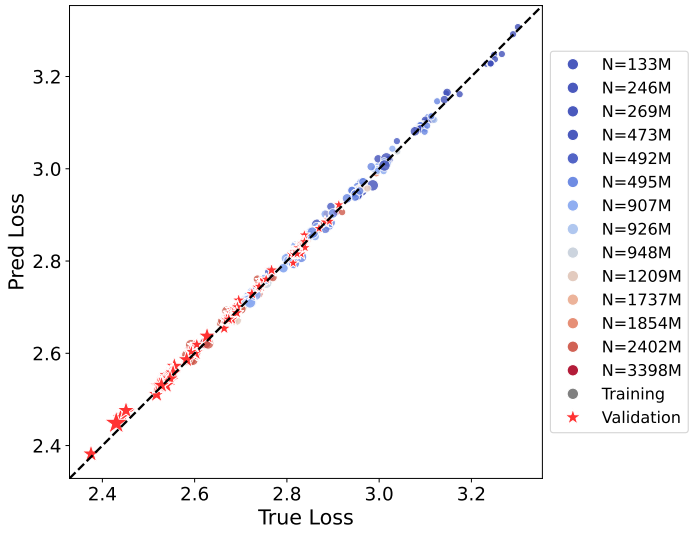

Figure 9: Fitting results of the scaling law of $L(N, D, N_a, G)$. Average validation loss error: 0.0083.

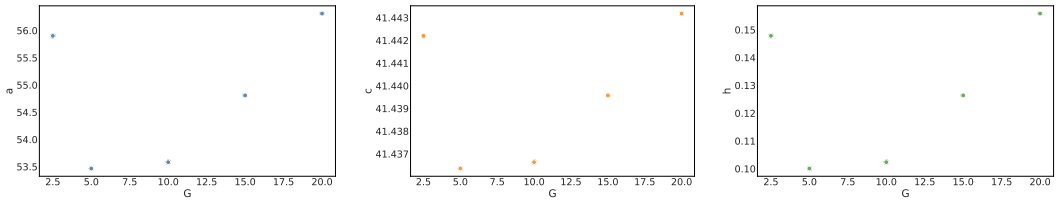

Figure 10: The correlations between a, c, h in Eq. 7 and G. a, c, h can be viewed as functions of G.

the structural properties of MoE architectures and reflects the impact of MoE architecture on performance. The results demonstrate that the scaling law which considers the structural factor G yields superior fitting performance. By analogy, to incorporate G into the scaling law $L(N, D, N_a, G)$, we first designed and conducted a series of controlled experiments where G was treated as the sole factor of variation, with all other factors held constant. Specifically, as G increases, the counts of routed experts and shared experts expand proportionally, whereas the corresponding expert dimensions shrink proportionally. Considering the marginal effect between G and loss, as well as the coupling relationships among G, N and N_a, we hypothesize that a, b, c and h—which appear in the numerator—are correlated with G. Experimental results demonstrate that the data size D is independent of G. The variation curves of the fitted hyperparameters a, c, h under different values of G are presented in Figure 10. Furthermore, we also provide the scaling law of validation loss with respect to G under other settings, which serve to observe the marginal effect of G.

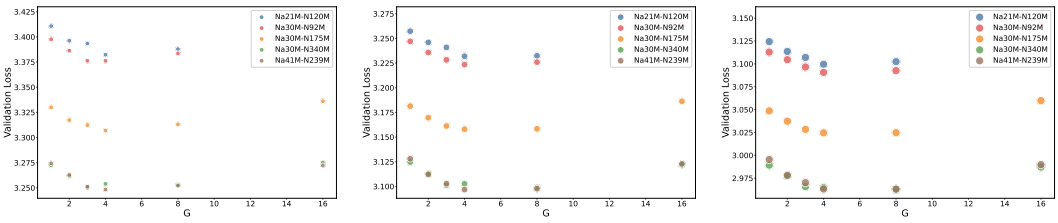

(a) Loss vs G with 10B data size. (b) Loss vs G with 20B data size. (c) Loss vs G with 50B data size.

Figure 11: Marginal effect of validation loss and G with $S = 0$. Data point sizes are proportional to D.

C.5 Fitting Results of the Scaling Law for $L(N, D, N_a, G, S)$

Similarly, the ratio of shared experts to activated experts (S) constitutes another critical structural characteristic of MoE architectures. The fitting performance of our final joint scaling law $L(N, D, N_a, G, S)$ is illustrated in Figure 12.

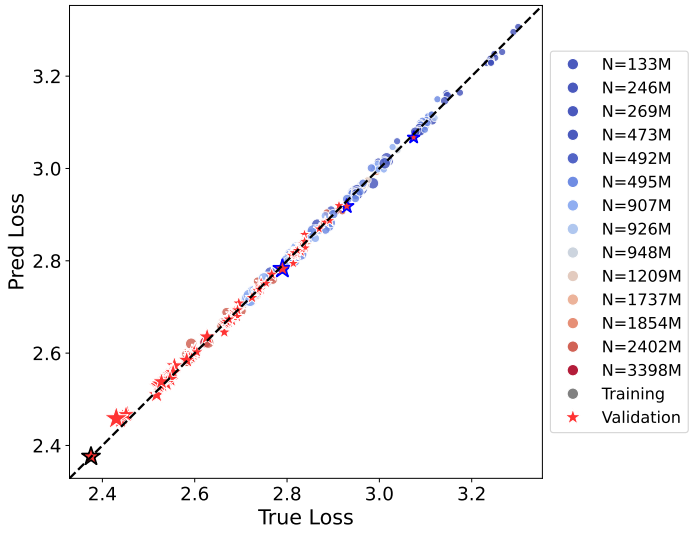

Figure 12: Fitting results of our final scaling law of $L(N, D, N_a, G, S)$. Average validation loss error: 0.0059.

Similarly, the analysis of hyperparameters related to S is presented in Figure 13. It can be observed: (1) m and n are independent of D, indicating that D and S are mutually decoupled; (2) m increases with the growth of N and N_a, whereas n decreases with the growth of N and N_a. Notably, the extreme point of S remains unchanged with variations in N and N_a; (3) ψ exhibits an obvious power-law relationship with N, N_a and D.

Furthermore, as stated in Section 4.5, the scaling law of S becomes increasingly prominent with the growth of model size. As shown in Figure 14.

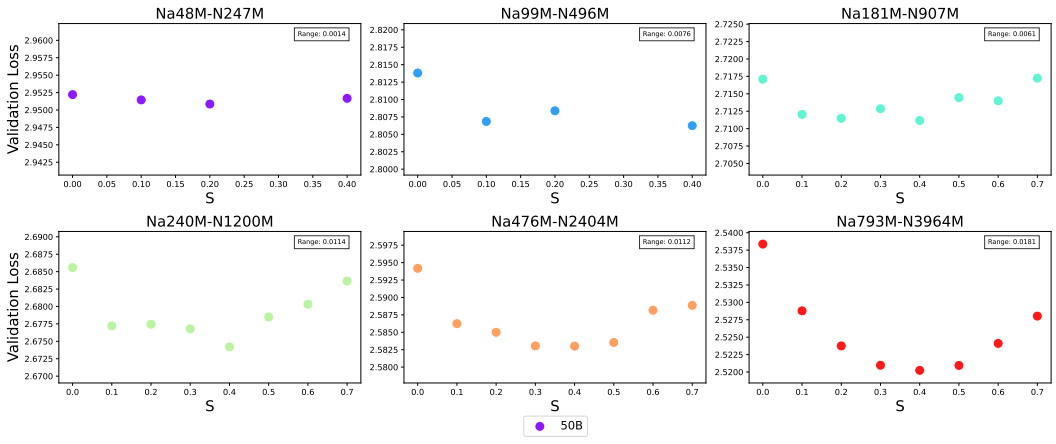

Figure 14: Illustration of the scaling law of S becoming increasingly prominent with growing model size with a data size of 50B.

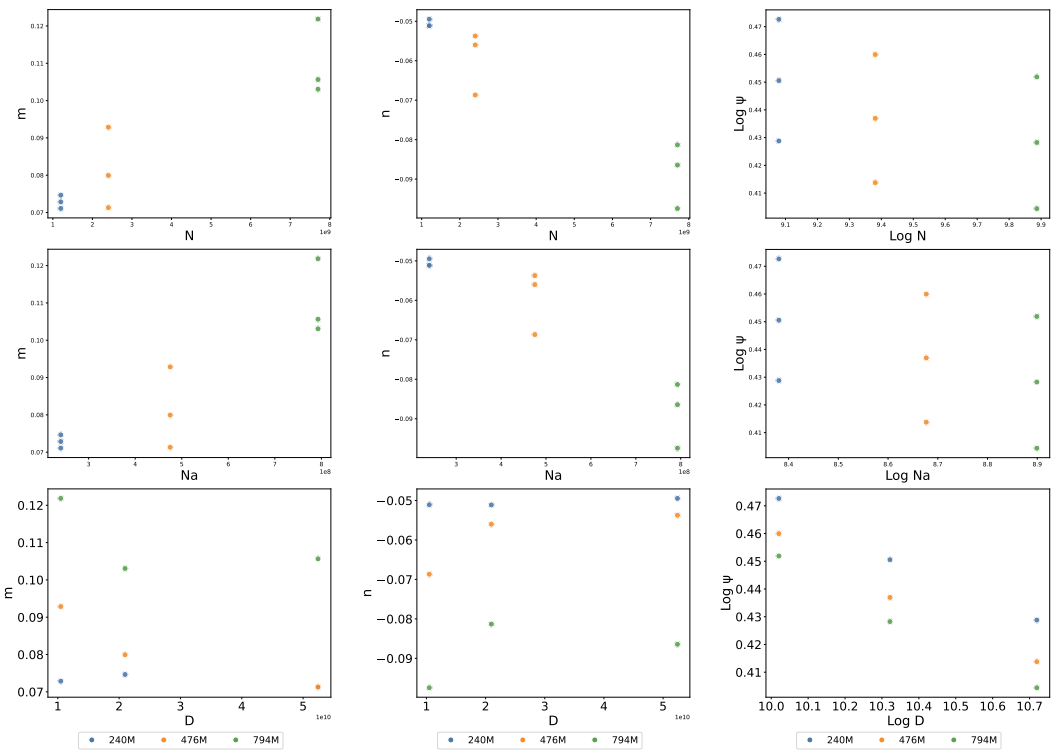

Figure 13: The correlations between m, n and ψ in Eq. 10 and N, N_a, D. m, n and ψ can be viewed as functions of N, N_a or D.

D Derivation of Theoretical Optimal G

First, we decompose $L(N, D, N_a, G, S)$ Eq. 15 into three components to isolate terms involving G. This decomposition leverages the fact that most variables (N, D, N_a, S) are independent of G:

$$L_{N,D,N_a,S}(G) = \underbrace{\left(eG + \frac{f}{G} + mS^2 + nS\right)}_{A(G)} \cdot \underbrace{\left(\frac{1}{N^\alpha} + \frac{k}{N_a^\alpha} + h\frac{N_a}{N}\right)}_{B} + \underbrace{\left(\frac{a}{N^\alpha} + \frac{c}{N_a^\alpha} + \frac{b}{D^\beta} + s\right)}_{C} = A(G) \cdot B + C \tag{16}$$

Compute $\frac{\partial L}{\partial G}$ and set to 0:

$$\frac{\partial L}{\partial G} = \left(e - \frac{f}{G^2}\right) \cdot B = 0 \tag{17}$$

Since $B \neq 0$, we get $e - \frac{f}{G^2} = 0$. Therefore:

$$G^2 = \frac{f}{e} \implies G = \sqrt{\frac{f}{e}} \quad (G > 0) \tag{18}$$

The second derivative checks to confirm a minimum.

$$\frac{\partial^2 L}{\partial G^2} = \frac{2f}{G^3} \cdot B > 0 \tag{19}$$

The extreme point (minimum) is:

$$G_{opt} = \sqrt{\frac{f}{e}} \tag{20}$$

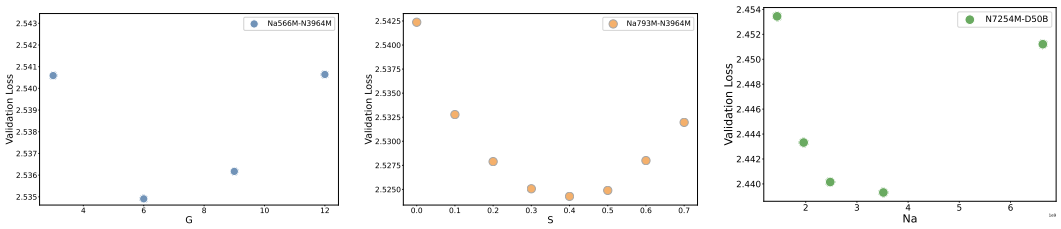

(a) G. (b) S. (c) N_a/N.

Figure 15: Verification of the marginal relationship for G, S and N_a/N under larger model sizes.

Substituting the optimized hyperparameters into the above Eq. 20 yields $G_{\text{opt}} \approx 6.78$.

To substantiate the validity of our conclusions, we conducted an analysis on the configurations of mainstream industrial MoE models, with detailed specifications in Table 3.

Table 3: Analyses of mainstream MoE models. Based on our scaling law, the theoretical optimal G and S are set as: $G \approx 6.78$, $S \approx 0.31$. The practical ranges provide relative recommended settings of G and S in practice with less effectiveness loss ($\leq$0.001).

Model	**G** (n_s**+TopK**)	**G (Actual)**	**G Practical Range (Thr** $= 0.001$**)**	**S (Actual)**	**S Practical Range (Thr** $= 0.001$**)**
gpt-oss-20b	$0+4$	4	$[5.09, 9.04]$	0	$[0.183, 0.446]$
Qwen3-30B-A3B	$0+8$	8	$[4.80, 9.58]$	0	$[0.156, 0.473]$
Hunyuan-A13B	$1+8$	9	$[4.99, 9.21]$	$1/9$	$[0.175, 0.455]$
GLM-4.5-Air	$1+8$	9	$[4.77, 9.64]$	$1/9$	$[0.154, 0.476]$
gpt-oss-120b	$0+4$	4	$[4.27, 10.77]$	0	$[0.102, 0.528]$
Qwen3-235B-A22B	$0+8$	8	$[4.61, 9.98]$	0	$[0.138, 0.492]$
GLM4.5	$1+8$	9	$[4.56, 10.09]$	$1/9$	$[0.133, 0.497]$
Deepseek-V3.1	$1+8$	9	$[4.20, 10.93]$	$1/9$	$[0.095, 0.535]$
Kimi-K2	$1+8$	9	$[3.85, 11.95]$	$1/9$	$[0.053, 0.577]$

Theoretically, the optimal values of G and S are determined to be 6.78 and 0.31, respectively. In practical deployment scenarios, however, a trade-off range for G and S is typically adopted, mainly owing to inherent efficiency constraints of MoE models. Building upon our proposed joint MoE scaling law, we further derive efficiency-aware ranges for G and S tailored to mainstream MoE models, with the loss threshold constrained to 0.001.

As presented in Table 3, the practical ranges of G exhibit a predominant distribution within the interval [4, 11] across diverse model configurations. Moreover, these practical ranges of G are demonstrated to be dependent on parameters N and N_a. Notably, the theoretically optimal value of G (i.e., 7) and our recommended practical range show strong consistency with the parameter settings of mainstream MoE models across varying model scales, which implicitly corroborates the validity of our inferences regarding G. The verification of the marginal effect for G under larger model sizes is illustrated in Figure 15(a).

E Derivation of Theoretical Optimal S

Analogous to the derivation of the optimal value of G, the isolation of S from other factors followed by the computation of its first-order derivative $\frac{\partial L}{\partial S}$—with the derivative set to 0:

$$\frac{\partial L}{\partial S} = (2mS + n) \cdot B = 0 \tag{21}$$

Since $B \neq 0$, we get $2mS + n = 0$. Therefore:

$$S_{opt} = -\frac{n}{2m} \tag{22}$$

Likewise, the second-derivative test confirms that S_{opt} corresponds to a minimum value. Substituting the optimized hyperparameters into the above Eq. 22 yields $S_{\text{opt}} \approx 0.31$.

Similarly, as shown in Table 3, we have also deduced the theoretical optimal value of S and its corresponding efficiency-aware practical range. It is of particular note that both our experimental findings and deductive inferences collectively highlight the indispensable role of shared experts in the design of MoE architectures.

Existing researches on the parameter S in mainstream models remain relatively insufficient. Most studies merely focus on the issue of whether to incorporate shared experts and no consistent consensus has been established in the field thus far. Our empirical findings demonstrate that the inclusion of S outperforms its exclusion in terms of model performance. Notably, within a specific range of S values, the model can consistently achieve satisfactory results with negligible performance fluctuations.

The verification of the marginal law for S under larger model sizes is illustrated in Figure 15(b).

F Derivation of Theoretical and Practical Optimal N_a/N

Theoretically Analysis. From Eq. 11, we can observe that there are two types of terms involving the activated model size N_a as a numerator or denominator. These two terms exert opposite effects on the loss of MoE models. Intuitively, this implies that there exists an optimal N_a given the configurations of other factors (e.g., the model size N). It has been experimentally validated on both the Torchtitan Liang et al. (2024) and Megatron Shoeybi et al. (2019) pre-training frameworks. To find the optimal point of $(\frac{N_a}{N})_{opt_t}$ in $L(N, D, N_a, G, S)$, firstly, let $r = \frac{N_a}{N}$, then decompose L as:

$$L_{N,D,G,S}(r) = \underbrace{\left(eG + \frac{f}{G} + mS^2 + nS\right)}_{A} \cdot \underbrace{\left(\frac{1}{N^\alpha} + \frac{k}{(rN)^\alpha} + hr\right)}_{B(r)} + \underbrace{\left(\frac{a}{N^\alpha} + \frac{c}{(rN)^\alpha} + \frac{b}{D^\beta} + s\right)}_{C(r)} \tag{23}$$

Compute first derivative $\frac{\partial L}{\partial r}$ and set to 0:

$$\frac{\partial L}{\partial r} = A \cdot \frac{\partial B}{\partial r} + \frac{\partial C}{\partial r} = 0 \tag{24}$$

Calculate partial derivatives:

$$\frac{\partial B}{\partial r} = -\frac{\alpha k}{N^\alpha r^{\alpha+1}} + h, \quad \frac{\partial C}{\partial r} = -\frac{\alpha c}{N^\alpha r^{\alpha+1}} \tag{25}$$

Substitute and simplify:

$$A\left(-\frac{\alpha k}{N^\alpha r^{\alpha+1}} + h\right) - \frac{\alpha c}{N^\alpha r^{\alpha+1}} = 0 \tag{26}$$

Rearrange terms to isolate r:

$$Ah = \frac{\alpha}{N^\alpha r^{\alpha+1}}(Ak + c) \implies r^{\alpha+1} = \frac{\alpha(Ak + c)}{AhN^\alpha} \tag{27}$$

Thus:

$$r = \left(\frac{\alpha(Ak + c)}{AhN^\alpha}\right)^{\frac{1}{\alpha+1}} \tag{28}$$

For $\alpha > 0$, $\frac{\partial^2 L}{\partial r^2} = \frac{\alpha(\alpha+1)(Ak+c)}{N^\alpha r^{\alpha+2}} > 0$, confirming a minimum.

Therefore, the optimal point of $(\frac{N_a}{N})_{opt_t}$ is:

$$\left(\frac{N_a}{N}\right)_{opt_t} = \left(\frac{\alpha \cdot \left[k \cdot \left(eG + \frac{f}{G} + mS^2 + nS\right) + c\right]}{hN^\alpha \cdot \left(eG + \frac{f}{G} + mS^2 + nS\right)}\right)^{\frac{1}{\alpha+1}} \tag{29}$$

From the expression of $\left(\frac{N_a}{N}\right)_{opt_t}$, it can be deduced that the theoretical optimal value is collectively determined by factors G, S and N. Specifically, G (refer to Appendix D) and S (refer to Appendix E), as validated by the foregoing analysis, generally exhibit respective independent optimal values. Therefore, the optimal $\left(\frac{N_a}{N}\right)_{opt_t}$ decreases as the model size N increases. It verifies that with the increasing total model sizes, the optimal MoE architecture will be sparser, which is consistent with the current trend of current industry-level MoE models (Kimi et al., 2025; OpenAI et al., 2025).

Practical Efficiency-aware Analysis. However, the theoretically optimal sparsity degree of MoE $\frac{N_a}{N}$ calculated in Eq. 29 cannot be directly used to guide the real-world MoE architecture design, for the efficiency of LLMs is also an essential factor. Specifically, when N_a gradually increases toward its optimal value, the performance gains become increasingly marginal, while the associated costs rise steadily. Therefore, it is necessary for us to explore the optimal $\frac{N_a}{N}$ under the consideration of the balance between performance gain and efficiency cost.

We define the loss gain threshold as ΔLoss for the step size of ΔN_a set as $0.01N$. As N_a is incrementally scaled according to the specified step size, the marginal gain of loss reduction will ultimately fall below the defined threshold ΔLoss, where we suppose the model reaches the practical efficiency-aware optimal $\frac{N_a}{N}$. The detailed derivation proceeds as follows:

Algorithm 1: Find Efficiency-aware Optimal N_a

Function `FindEfficiencyAwareNa` (N, D, G, S, *threshold*) **:**

```
step = 0.01 × N;
N_a_prev ← step;
loss_prev ← L(N, D, N_a_prev, G, S);
iteration = 1;
max_iterations = n;
while iteration ≤ max_iterations do
    N_a_current ← N_a_prev + step;
    loss_current ← L(N, D, N_a_current, G, S);
    loss_reduction ← loss_prev − loss_current;
    if loss_reduction < threshold then
        return N_a_current;
    N_a_prev ← N_a_current;
    loss_prev ← loss_current;
    iteration ← iteration + 1;
return None;
```

Hence, for a given model size N, our MoE scaling law yields a practically applicable range for N_a, i.e., spanning the interval from the practical efficiency-aware optimal point to the theoretically optimal point, i.e., $N_a \in [\left(\frac{N_a}{N}\right)_{opt_e}, \left(\frac{N_a}{N}\right)_{opt_t}]$.

To substantiate the validity of our conclusions, we conducted an analysis on the configurations of mainstream industrial MoE models, with detailed specifications in Table 4. It indicates that the activated model sizes N_a of most mainstream MoE models are consistent with our recommended ranges above. Practical MoE designs could jointly consider both effectiveness and efficiency with the help of our proposed MoE scaling laws. The verification of the marginal law for N_a/N under larger model sizes is illustrated in Figure 15(c).

Discussion on the Optimal G and N_a. We attempt to explain possible misunderstandings that the phenomenon reflected by our MoE scaling law (i.e., G and N_a have optimal value) seems to "conflict with" our intuitive cognition on expanding MoE experts or activated parameters (i.e., larger G and N_a are likely to achieve better results). Precisely, it intuitively seems that larger values of G and N_a would be preferable. This notion, however, does not contradict our proposed MoE scaling law: typically, when adjusting N_a while keeping the total model size N fixed (which is the most natural operation of "increasing N_a"), such adjustment is achieved by increasing G, leading to the concurrent growth of both parameters N_a and G. In this situation, our formula correctly reflects that the loss generally decreases under these circumstances. Nevertheless, when focusing on G with other factors held constant, increasing G results in a greater number of routed experts but progressively

Table 4: Theoretical and practical efficiency-aware optimal N_a/N analysis for mainstream MoE models

Model	Na-N (Actual)	Na/N Theoretical Opt	Na/N Practical Opt (ΔLoss $= 0.001$)	Na/N Practical Opt (ΔLoss $= 0.005$)
gpt-oss-20b	3.6B-21B	42.89% (9.0B)	22.00% (4.6B)	9.00% (1.9B)
Qwen3-30B-A3B	3B-30B	40.04% (12.0B)	21.00% (6.3B)	9.00% (2.7B)
Hunyuan-A13B	13B-80B	33.16% (26.5B)	18.00% (14.4B)	7.00% (5.6B)
GLM-4.5-Air	12B-106B	31.41% (33.3B)	17.00% (18.0B)	7.00% (7.4B)
gpt-oss-120b	5.1B-117B	30.82% (36.1B)	16.00% (18.7B)	7.00% (8.2B)
Qwen3-235B-A22B	22B-235B	26.95% (63.33B)	14.00% (32.9B)	6.00% (14.1B)
GLM-4.5	32B-355B	24.89% (88.4B)	13.00% (46.2B)	6.00% (21.3B)
Deepseek-V3.1	37B-671B	22.02% (147.8B)	12.00% (80.5B)	5.00% (33.6B)
Kimi-K2	32B-1T	20.40% (204.0B)	11.00% (110.0B)	5.00% (50.0B)

smaller expert dimensions due to partitioning. While appropriate fine-grained partitioning can enhance performance, exceeding a specific threshold will conversely impair model performance. Similarly, when focusing on N_a with other factors fixed, increasing N_a leads to larger expert dimensions but a reduced number of all/routed experts, thereby diminishing the sparsity advantage of the MoE model. This induces gradual structural distortion in the MoE architecture, which in turn disrupts the advantage of MoE's combinational activation mechanism and thus degrades performance.

G Compute-Optimality with Fixed Configurations

We controll the total computation cost $C = D \cdot N_a$ and analyze the relationship between the optimal loss and C. According to our Implications #1 and #2, G and S have optimal values. Thus, the term $eG + \frac{f}{G} + mS^2 + nS$ can be expressed as a constant term $const$ under the optimal configuration. When N is fixed, substituting $D = \frac{C}{N_a}$ into our joint MoE scaling law (Eq. 11) yields the following result:

$$\begin{gathered} L(N_a, C) = C_0 + (const \cdot k + c) \cdot \frac{1}{N_a^{\alpha}} + \frac{const \cdot h}{N} \cdot N_a + \frac{bN_a^{\beta}}{C^{\beta}} \\ \text{where } const = eG + \frac{f}{G} + mS^2 + nS \text{ and } C_0 = \frac{const + a}{N^{\alpha}} + s. \end{gathered} \tag{30}$$

To find the optimal N_a (denoted N_a^*) that minimizes $L(N_a)$, compute the first derivative of $L(N_a)$ with respect to N_a and set $\frac{dL}{dN_a} = 0$:

$$\frac{b\beta N_a^{*\beta-1}}{C^{\beta}} = \alpha \left(const \cdot k + c\right) N_a^{*-\alpha-1} - \frac{const \cdot h}{N} \tag{31}$$

Substitute N_a^* into Eq. 30 to get the optimal loss L^*:

$$\begin{gathered} L^*(C) = C_0 + \frac{(const \cdot k + c)(\alpha + \beta)}{\beta} N_a^{*-\alpha} + \frac{const \cdot h(\beta - 1)}{N\beta} N_a^*, \\ \text{subject to } \frac{b\beta N_a^{*\beta-1}}{C^{\beta}} = \alpha \left(const \cdot k + c\right) N_a^{*-\alpha-1} - \frac{const \cdot h}{N}, \\ \text{where } const = eG + \frac{f}{G} + mS^2 + nS \text{ and } C_0 = \frac{const + a}{N^{\alpha}} + s. \end{gathered} \tag{32}$$

To facilitate understanding, we conduct the derivation under the predefined fixed configuration: $G = 7$, $S = 0.31$ and $N = 1$T. The expression for $L^*(C)$ is provided as follows and illustrated in Figure 16:

$$L^*(C) \approx 1.87 + 576 \cdot C^{-0.158} \tag{33}$$

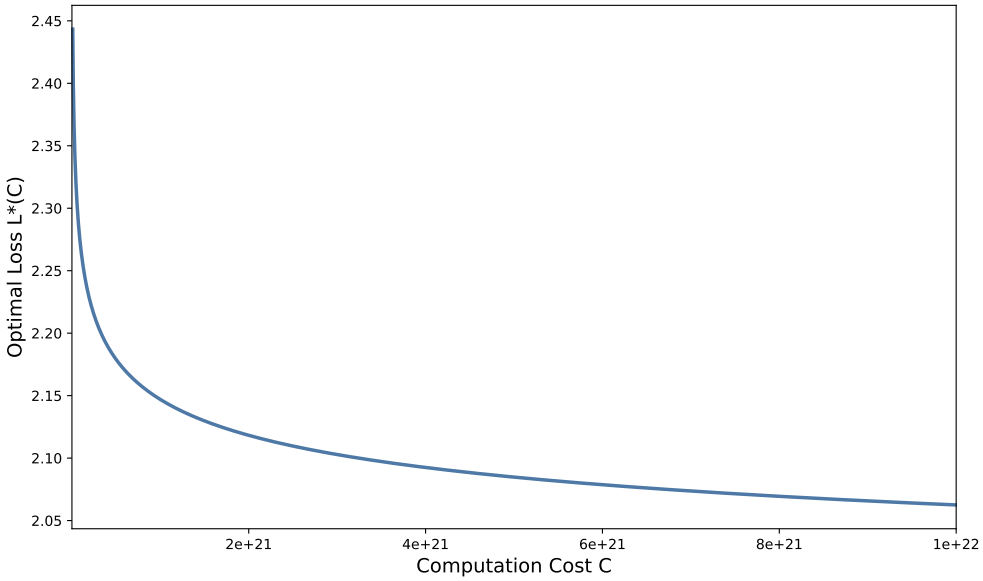

Figure 16: Illustration of $L^*(C)$ under the configuration of $N = 1\text{T}$, $G = 7$ and $S = 0.31$.

H Derivation of the u-v Relationship For N_a

To achieve the exclusive variation of the control variable N_a, it can be derived from Eq. 3 that when G and S are fixed, N_a needs to be adjusted by modifying the expert dimension and the number of routed experts. Specifically, we scaled the expert dimension by a factor of u while scaling down the number of routed experts by a corresponding factor v. However, to ensure that N remains unchanged simultaneously, the following constraint applies:

$$\big(4d_{\text{head}} \cdot n_h + 3d_{\text{expert}}(SG + n_e)\big)d_{\text{hidden}} \cdot l = \big(4d_{\text{head}} \cdot n_h + 3d_{\text{expert}} \cdot u(SG + n_e \cdot v)\big)d_{\text{hidden}} \cdot l \quad (34)$$

Through formula transformation, we can derive:

$$v = \frac{(1-u) \cdot S \cdot G + n_e}{u \cdot n_e}. \quad (35)$$

Thus, by setting the ratio of u to v according to the aforementioned Eq. 35, the controlled variation of N_a can be achieved. For instance, when $N = 2.4\text{B}$, $G = 20$ and $S = 0.2$, N_a takes values in the set $\{303\text{M}, 476\text{M}, 819\text{M}, 1507\text{M}, 2196\text{M}\}$, with the corresponding d_{expert} being $\{112, 224, 448, 896, 1344\}$ and the respective n_e being $\{260, 128, 62, 29, 18\}$.

I Related Scaling Laws

Table 5: Comparison with existing MoE scaling laws.

	N	Na	D	G	S
Scaling Laws for Fine-Grained MoE (Krajewski et al., 2024)	✓	✗	✓	✓	✗
Parameters vs. FLOPs (Abnar et al., 2025)	✓	✓	✓	✗	✗
Joint MoE Scaling Laws (Ludziejewski et al., 2025)	✓	✓	✓	✗	✗
Scaling Laws Across Architectures (Wang et al., 2024b)	✓	✗	✓	✗	✗
Unified Routed LMs (Clark et al., 2022)	✓	✗	✗	✗	✗
Our MoE Scaling Law	✓	✓	✓	✓	✓

We selected two related scaling laws for comparison, each focusing on different aspects. Below, we briefly introduce their main ideas and describe how we use them to compare with the scaling law derived from our experiments.

I.1 Scaling Laws for Fine-Grained Mixture-of-Experts

Krajewski et al. (2024) introduced a *granularity* factor into MoE scaling laws. They model the training loss $\mathcal{L}$ as a function of the number of **active parameters** N, the dataset size D and the **granularity** G:

$$\mathcal{L}(N, D, G) = c + \left(\frac{g}{G^{\gamma}} + a\right)\frac{1}{N^{\alpha}} + \frac{b}{D^{\beta}}. \tag{36}$$

Here c is the irreducible loss. The term $N^{-\alpha}$ captures the effect of model size, adjusted by G: finer experts (larger G) reduce this contribution. The last term $D^{-\beta}$ reflects the improvement from more data. Overall, the law indicates diminishing returns from N and D, with better performance at higher G. As shown in Figure 5, this fitted result is less accurate than ours. The detailed fitted constants and values in Eq. 36 are presented below in Table 6.

Table 6: Fitted constants and their values in Eq. 36.

Constant	Value
a	81.9404
α	0.2380
b	3195.7723
β	0.3695
c	1.7709
g	0.0004
γ	0.0028

I.2 Scaling Laws for Optimal Sparsity in MoE

Abnar et al. (2025) analyzed the effect of **sparsity** S, defined as the fraction of inactive experts. Their scaling law is:

$$L(N, D, S) = \frac{a}{N^{\alpha}} + \frac{b}{D^{\beta}} + \frac{c}{(1-S)^{\lambda}} + \frac{d}{(1-S)^{\delta}\, N^{\gamma}} + e. \tag{37}$$

The first two terms represent the standard effects of model and data size. The third term penalizes high sparsity, while the fourth couples sparsity with model size. The constant e is an offset. This form shows that both the level of sparsity and its interaction with N influence the loss. As shown in Figure 5, our method achieves a better fit than this result. The detailed fitted constants and values in Eq. 37 are presented below in Table 7.

Table 7: Fitted constants and their values in Eq. 37.

Constant	Value
a	43.2889
α	0.1948
b	8280.7176
β	0.4145
e	1.6351
c	0.0003
d	9.4982
λ	1.8469
δ	0.0802
γ	14.0591

I.3 Comparison Methodology

For a fair comparison, we use the same dataset to fit as ours for these scaling laws. Each formula is applied without modification and parameters are optimized on identical experimental results under the same settings. This ensures that any differences arise solely from the functional forms. In

addition, we also fit other MoE scaling law (Ludziejewski et al., 2025; Clark et al., 2022), but their performance is likewise inferior to ours. This is likely because our formulation incorporates a more comprehensive set of MoE factors—D, N, N_a, G, S—and is applied over a broader range of MoE settings. Furthermore, our fitting carefully accounts for marginal effects while leveraging Occam's razor to simplify both hyperparameters and functional forms.

J LIMITATIONS

Our work has several limitations. In this work, we mainly focus on the classical MoE architecture. The analysis has not been validated at extremely larger scales or with alternative MoE architectures / training objectives due to the resource limit. In addition, we focus primarily on MoE-related factors and do not examine other components of LLMs that may also impact the performance of MoE, such as the attention layers and their interactions. Future work should extend the analysis to broader architectures and assess robustness.

K VARIATION OF DIFFERENT FACTORS

In our study, the core factors, including N_a, N, G, and S, are varied in strict adherence to the principle of controlling variables. We have already discussed the methods used to control these factors during the experiments in Appendix C. To clarify the experimental procedure, we provide a series of illustrations in Figure 17 that demonstrate how each variable is systematically adjusted:

L DETAILED SETTINGS OF EXPERIMENTS

We show the detailed configurations of our experiments as follows. Precisely, the value ranges of various factors in the experimental setup are as follows: for fitting data points, $G \in (1, 20]$, $S \in [0.0, 0.8]$, $N_a \in [30\text{M}, 2.2\text{B}]$, $N \in [133\text{M}, 3.4\text{B}]$ and $D \in [10\text{B}, 50\text{B}]$; for validation data points, $G \in (1, 40]$, $S \in [0.0, 0.7]$, $N_a \in [453\text{M}, 6.6\text{B}]$, $N \in [2.4\text{B}, 30\text{B}]$ and $D \in [10\text{B}, 100\text{B}]$.

We should highlight that our joint MoE scaling law is designed to accommodate practical experimental configurations. Therefore, the MoE configurations are more focused on the relatively practical settings, with partial of extreme settings to reveal the marginal effect of different factors. For the validation data, we adopt larger model/data sizes and broader ranges of factors to evaluate the effectiveness of our scaling law. For some uncommon and impractical experimental setups, such as those with extremely large G and exceptionally high N_a/N ratios simultaneously (whose efficiency is unsatisfactory in the view of MoE models), perfect fitting is not pursued by our MoE scaling law. The detailed configurations are given in Table 8.

Table 8: All configurations of experiments. The last column is **Label**, where ✓ indicates that the data point is used for validation and ✗ indicates that the data point is used for fitting or for observing marginal patterns.

	Na	N	D	G	S	Label		Na	N	D	G	S	Label
0	48M	247M	10B	2.5	0.2	✗	1	48M	247M	10B	5	0.2	✗
2	48M	247M	10B	10	0.2	✗	3	48M	247M	10B	15	0.2	✗
4	48M	247M	10B	20	0.2	✗	5	48M	247M	20B	2.5	0.2	✗
6	48M	247M	20B	5	0.2	✗	7	48M	247M	20B	10	0.2	✗
8	48M	247M	20B	15	0.2	✗	9	48M	247M	20B	20	0.2	✗
10	48M	247M	50B	2.5	0.2	✗	11	48M	247M	50B	5	0.2	✗
12	48M	247M	50B	10	0.2	✗	13	48M	247M	50B	15	0.2	✗
14	48M	247M	50B	20	0.2	✗	15	99M	496M	10B	2.5	0.2	✗
16	99M	496M	10B	5	0.2	✗	17	99M	496M	10B	10	0.2	✗
18	99M	496M	10B	15	0.2	✗	19	99M	496M	10B	20	0.2	✗
20	99M	496M	20B	2.5	0.2	✗	21	99M	496M	20B	5	0.2	✗
22	99M	496M	20B	10	0.2	✗	23	99M	496M	20B	15	0.2	✗

Continued on next page

Table 8 continued from previous page

	Na	N	D	G	S	Label		Na	N	D	G	S	Label
24	99M	496M	20B	20	0.2	✗	25	99M	496M	50B	2.5	0.2	✗
26	99M	496M	50B	5	0.2	✗	27	99M	496M	50B	10	0.2	✗
28	99M	496M	50B	15	0.2	✗	29	99M	496M	50B	20	0.2	✗
30	181M	907M	10B	2.5	0.2	✗	31	181M	907M	10B	5	0.2	✗
32	181M	907M	10B	10	0.2	✗	33	181M	907M	10B	15	0.2	✗
34	181M	907M	10B	20	0.2	✗	35	181M	907M	20B	2.5	0.2	✗
36	181M	907M	20B	5	0.2	✗	37	181M	907M	20B	10	0.2	✗
38	181M	907M	20B	15	0.2	✗	39	181M	907M	20B	20	0.2	✗
40	181M	907M	50B	2.5	0.2	✗	41	181M	907M	50B	5	0.2	✗
42	181M	907M	50B	10	0.2	✗	43	181M	907M	50B	15	0.2	✗
44	181M	907M	50B	20	0.2	✗	45	48M	133M	10B	10	0.2	✗
46	48M	247M	10B	10	0.2	✗	47	48M	473M	10B	10	0.2	✗
48	48M	926M	10B	10	0.2	✗	49	48M	133M	20B	10	0.2	✗
50	48M	247M	20B	10	0.2	✗	51	48M	473M	20B	10	0.2	✗
52	48M	926M	20B	10	0.2	✗	53	48M	133M	50B	10	0.2	✗
54	48M	247M	50B	10	0.2	✗	55	48M	473M	50B	10	0.2	✗
56	48M	926M	50B	10	0.2	✗	57	99M	269M	10B	10	0.2	✗
58	99M	496M	10B	10	0.2	✗	59	99M	949M	10B	10	0.2	✗
60	99M	1855M	10B	10	0.2	✗	61	99M	269M	20B	10	0.2	✗
62	99M	496M	20B	10	0.2	✗	63	99M	949M	20B	10	0.2	✗
64	99M	1855M	20B	10	0.2	✗	65	99M	269M	50B	10	0.2	✗
66	99M	496M	50B	10	0.2	✗	67	99M	949M	50B	10	0.2	✗
68	99M	1855M	50B	10	0.2	✗	69	181M	492M	10B	10	0.2	✗
70	181M	907M	10B	10	0.2	✗	71	181M	1738M	10B	10	0.2	✗
72	181M	3399M	10B	10	0.2	✗	73	181M	492M	20B	10	0.2	✗
74	181M	907M	20B	10	0.2	✗	75	181M	1738M	20B	10	0.2	✗
76	181M	3399M	20B	10	0.2	✗	77	181M	492M	50B	10	0.2	✗
78	181M	907M	50B	10	0.2	✗	79	181M	1738M	50B	10	0.2	✗
80	181M	3399M	50B	10	0.2	✗	81	48M	247M	10B	10	0.0	✗
82	48M	247M	10B	10	0.1	✗	83	48M	247M	10B	10	0.2	✗
84	48M	247M	10B	10	0.4	✗	85	48M	247M	20B	10	0.0	✗
86	48M	247M	20B	10	0.1	✗	87	48M	247M	20B	10	0.2	✗
88	48M	247M	20B	10	0.4	✗	89	48M	247M	50B	10	0.0	✗
90	48M	247M	50B	10	0.1	✗	91	48M	247M	50B	10	0.2	✗
92	48M	247M	50B	10	0.4	✗	93	99M	496M	10B	10	0.0	✗
94	99M	496M	10B	10	0.1	✗	95	99M	496M	10B	10	0.2	✗
96	99M	496M	10B	10	0.4	✗	97	99M	496M	20B	10	0.0	✗
98	99M	496M	20B	10	0.1	✗	99	99M	496M	20B	10	0.2	✗
100	99M	496M	20B	10	0.4	✗	101	99M	496M	50B	10	0.0	✗
102	99M	496M	50B	10	0.1	✗	103	99M	496M	50B	10	0.2	✗
104	99M	496M	50B	10	0.4	✗	105	181M	907M	10B	10	0.0	✗
106	181M	907M	10B	10	0.1	✗	107	181M	907M	10B	10	0.2	✗
108	181M	907M	10B	10	0.3	✗	109	181M	907M	10B	10	0.4	✗
110	181M	907M	10B	10	0.5	✗	111	181M	907M	10B	10	0.6	✗
112	181M	907M	10B	10	0.7	✗	113	181M	907M	20B	10	0.0	✗
114	181M	907M	20B	10	0.1	✗	115	181M	907M	20B	10	0.2	✗
116	181M	907M	20B	10	0.3	✗	117	181M	907M	20B	10	0.4	✗
118	181M	907M	20B	10	0.5	✗	119	181M	907M	20B	10	0.6	✗
120	181M	907M	20B	10	0.7	✗	121	181M	907M	50B	10	0.0	✗
122	181M	907M	50B	10	0.1	✗	123	181M	907M	50B	10	0.2	✗
124	181M	907M	50B	10	0.3	✗	125	181M	907M	50B	10	0.4	✗
126	181M	907M	50B	10	0.5	✗	127	181M	907M	50B	10	0.6	✗
128	181M	907M	50B	10	0.7	✗	129	240M	1209M	10B	10	0.0	✗
130	240M	1209M	10B	10	0.1	✗	131	240M	1209M	10B	10	0.2	✗
132	240M	1209M	10B	10	0.3	✗	133	240M	1209M	10B	10	0.4	✗

Continued on next page

Table 8 continued from previous page

	Na	N	D	G	S	Label		Na	N	D	G	S	Label
134	240M	1209M	10B	10	0.5	✗	135	240M	1209M	10B	10	0.6	✗
136	240M	1209M	10B	10	0.7	✗	137	240M	1209M	20B	10	0.0	✗
138	240M	1209M	20B	10	0.1	✗	139	240M	1209M	20B	10	0.2	✗
140	240M	1209M	20B	10	0.3	✗	141	240M	1209M	20B	10	0.4	✗
142	240M	1209M	20B	10	0.5	✗	143	240M	1209M	20B	10	0.6	✗
144	240M	1209M	20B	10	0.7	✗	145	240M	1209M	50B	10	0.0	✗
146	240M	1209M	50B	10	0.1	✗	147	240M	1209M	50B	10	0.2	✗
148	240M	1209M	50B	10	0.3	✗	149	240M	1209M	50B	10	0.4	✗
150	240M	1209M	50B	10	0.5	✗	151	240M	1209M	50B	10	0.6	✗
152	240M	1209M	50B	10	0.7	✗	153	476M	2404M	10B	10	0.0	✗
154	476M	2404M	10B	10	0.1	✗	155	476M	2404M	10B	10	0.3	✗
156	476M	2404M	10B	10	0.4	✗	157	476M	2404M	10B	10	0.5	✗
158	476M	2404M	10B	10	0.6	✗	159	476M	2404M	10B	10	0.7	✗
160	476M	2404M	20B	10	0.0	✗	161	476M	2404M	20B	10	0.1	✗
162	476M	2404M	20B	10	0.3	✗	163	476M	2404M	20B	10	0.4	✗
164	476M	2404M	20B	10	0.5	✗	165	476M	2404M	20B	10	0.6	✗
166	476M	2404M	20B	10	0.7	✗	167	476M	2404M	50B	10	0.0	✗
168	476M	2404M	50B	10	0.1	✗	169	476M	2404M	50B	10	0.3	✗
170	476M	2404M	50B	10	0.4	✗	171	476M	2404M	50B	10	0.5	✗
172	476M	2404M	50B	10	0.6	✗	173	476M	2404M	50B	10	0.7	✗
174	240M	1209M	10B	5	0.0	✗	175	240M	1209M	10B	5	0.2	✗
176	240M	1209M	10B	5	0.4	✗	177	240M	1209M	10B	5	0.6	✗
178	240M	1209M	10B	5	0.8	✗	179	240M	1209M	20B	5	0.0	✗
180	240M	1209M	20B	5	0.2	✗	181	240M	1209M	20B	5	0.4	✗
182	240M	1209M	20B	5	0.6	✗	183	240M	1209M	20B	5	0.8	✗
184	240M	1209M	50B	5	0.0	✗	185	240M	1209M	50B	5	0.2	✗
186	240M	1209M	50B	5	0.4	✗	187	240M	1209M	50B	5	0.6	✗
188	240M	1209M	50B	5	0.8	✗	189	476M	2404M	10B	5	0.0	✗
190	476M	2404M	10B	5	0.2	✗	191	476M	2404M	10B	5	0.4	✗
192	476M	2404M	10B	5	0.6	✗	193	476M	2404M	10B	5	0.8	✗
194	476M	2404M	20B	5	0.0	✗	195	476M	2404M	20B	5	0.2	✗
196	476M	2404M	20B	5	0.4	✗	197	476M	2404M	20B	5	0.6	✗
198	476M	2404M	20B	5	0.8	✗	199	476M	2404M	50B	5	0.0	✗
200	476M	2404M	50B	5	0.2	✗	201	476M	2404M	50B	5	0.4	✗
202	476M	2404M	50B	5	0.6	✗	203	476M	2404M	50B	5	0.8	✗
204	31M	247M	10B	20	0.2	✗	205	31M	247M	20B	20	0.2	✗
206	31M	247M	30B	20	0.2	✗	207	31M	247M	50B	20	0.2	✗
208	64M	496M	10B	20	0.2	✗	209	99M	496M	10B	20	0.2	✗
210	170M	496M	10B	20	0.2	✗	211	312M	496M	10B	20	0.2	✗
212	453M	496M	10B	20	0.2	✗	213	64M	496M	20B	20	0.2	✗
214	99M	496M	20B	20	0.2	✗	215	170M	496M	20B	20	0.2	✗
216	312M	496M	20B	20	0.2	✗	217	453M	496M	20B	20	0.2	✗
218	64M	496M	30B	20	0.2	✗	219	99M	496M	30B	20	0.2	✗
220	170M	496M	30B	20	0.2	✗	221	312M	496M	30B	20	0.2	✗
222	453M	496M	30B	20	0.2	✗	223	64M	496M	50B	20	0.2	✗
224	99M	496M	50B	20	0.2	✗	225	170M	496M	50B	20	0.2	✗
226	312M	496M	50B	20	0.2	✗	227	453M	496M	50B	20	0.2	✗
228	116M	907M	10B	20	0.2	✗	229	181M	907M	10B	20	0.2	✗
230	310M	907M	10B	20	0.2	✗	231	570M	907M	10B	20	0.2	✗
232	829M	907M	10B	20	0.2	✗	233	116M	907M	20B	20	0.2	✗
234	181M	907M	20B	20	0.2	✗	235	310M	907M	20B	20	0.2	✗
236	570M	907M	20B	20	0.2	✗	237	829M	907M	20B	20	0.2	✗
238	116M	907M	30B	20	0.2	✗	239	181M	907M	30B	20	0.2	✗
240	310M	907M	30B	20	0.2	✗	241	570M	907M	30B	20	0.2	✗
242	829M	907M	30B	20	0.2	✗	243	116M	907M	50B	20	0.2	✗

Continued on next page

Table 8 continued from previous page

	Na	N	D	G	S	Label		Na	N	D	G	S	Label
244	181M	907M	50B	20	0.2	✗	245	310M	907M	50B	20	0.2	✗
246	570M	907M	50B	20	0.2	✗	247	829M	907M	50B	20	0.2	✗
248	304M	2404M	10B	20	0.2	✗	249	476M	2404M	10B	20	0.2	✗
250	820M	2404M	10B	20	0.2	✗	251	1508M	2404M	10B	20	0.2	✗
252	2196M	2404M	10B	20	0.2	✗	253	304M	2404M	20B	20	0.2	✗
254	476M	2404M	20B	20	0.2	✗	255	820M	2404M	20B	20	0.2	✗
256	1508M	2404M	20B	20	0.2	✗	257	2196M	2404M	20B	20	0.2	✗
258	304M	2404M	30B	20	0.2	✗	259	476M	2404M	30B	20	0.2	✗
260	820M	2404M	30B	20	0.2	✗	261	1508M	2404M	30B	20	0.2	✗
262	2196M	2404M	30B	20	0.2	✗	263	304M	2404M	50B	20	0.2	✗
264	476M	2404M	50B	20	0.2	✗	265	820M	2404M	50B	20	0.2	✗
266	1508M	2404M	50B	20	0.2	✗	267	2196M	2404M	50B	20	0.2	✗
268	22M	121M	10B	1	0.0	✗	269	22M	121M	10B	2	0.0	✗
270	22M	121M	10B	3	0.0	✗	271	22M	121M	10B	4	0.0	✗
272	22M	121M	10B	8	0.0	✗	273	22M	121M	10B	16	0.0	✗
274	22M	121M	20B	1	0.0	✗	275	22M	121M	20B	2	0.0	✗
276	22M	121M	20B	3	0.0	✗	277	22M	121M	20B	4	0.0	✗
278	22M	121M	20B	8	0.0	✗	279	22M	121M	20B	16	0.0	✗
280	22M	121M	50B	1	0.0	✗	281	22M	121M	50B	2	0.0	✗
282	22M	121M	50B	3	0.0	✗	283	22M	121M	50B	4	0.0	✗
284	22M	121M	50B	8	0.0	✗	285	22M	121M	50B	16	0.0	✗
286	30M	93M	10B	1	0.0	✗	287	30M	93M	10B	2	0.0	✗
288	30M	93M	10B	3	0.0	✗	289	30M	93M	10B	4	0.0	✗
290	30M	93M	10B	8	0.0	✗	291	30M	93M	10B	16	0.0	✗
292	30M	93M	20B	1	0.0	✗	293	30M	93M	20B	2	0.0	✗
294	30M	93M	20B	3	0.0	✗	295	30M	93M	20B	4	0.0	✗
296	30M	93M	20B	8	0.0	✗	297	30M	93M	20B	16	0.0	✗
298	30M	93M	50B	1	0.0	✗	299	30M	93M	50B	2	0.0	✗
300	30M	93M	50B	3	0.0	✗	301	30M	93M	50B	4	0.0	✗
302	30M	93M	50B	8	0.0	✗	303	30M	93M	50B	16	0.0	✗
304	30M	175M	10B	1	0.0	✗	305	30M	175M	10B	2	0.0	✗
306	30M	175M	10B	3	0.0	✗	307	30M	175M	10B	4	0.0	✗
308	30M	175M	10B	8	0.0	✗	309	30M	175M	10B	16	0.0	✗
310	30M	175M	20B	1	0.0	✗	311	30M	175M	20B	2	0.0	✗
312	30M	175M	20B	3	0.0	✗	313	30M	175M	20B	4	0.0	✗
314	30M	175M	20B	8	0.0	✗	315	30M	175M	20B	16	0.0	✗
316	30M	175M	50B	1	0.0	✗	317	30M	175M	50B	2	0.0	✗
318	30M	175M	50B	3	0.0	✗	319	30M	175M	50B	4	0.0	✗
320	30M	175M	50B	8	0.0	✗	321	30M	175M	50B	16	0.0	✗
322	30M	340M	10B	1	0.0	✗	323	30M	340M	10B	2	0.0	✗
324	30M	340M	10B	3	0.0	✗	325	30M	340M	10B	4	0.0	✗
326	30M	340M	10B	8	0.0	✗	327	30M	340M	10B	16	0.0	✗
328	30M	340M	20B	1	0.0	✗	329	30M	340M	20B	2	0.0	✗
330	30M	340M	20B	3	0.0	✗	331	30M	340M	20B	4	0.0	✗
332	30M	340M	20B	8	0.0	✗	333	30M	340M	20B	16	0.0	✗
334	30M	340M	50B	1	0.0	✗	335	30M	340M	50B	2	0.0	✗
336	30M	340M	50B	3	0.0	✗	337	30M	340M	50B	4	0.0	✗
338	30M	340M	50B	8	0.0	✗	339	30M	340M	50B	16	0.0	✗
340	41M	239M	10B	1	0.0	✗	341	41M	239M	10B	2	0.0	✗
342	41M	239M	10B	3	0.0	✗	343	41M	239M	10B	4	0.0	✗
344	41M	239M	10B	8	0.0	✗	345	41M	239M	10B	16	0.0	✗
346	41M	239M	20B	1	0.0	✗	347	41M	239M	20B	2	0.0	✗
348	41M	239M	20B	3	0.0	✗	349	41M	239M	20B	4	0.0	✗
350	41M	239M	20B	8	0.0	✗	351	41M	239M	20B	16	0.0	✗
352	41M	239M	50B	1	0.0	✗	353	41M	239M	50B	2	0.0	✗

Continued on next page

Table 8 continued from previous page

	Na	N	D	G	S	Label		Na	N	D	G	S	Label
354	41M	239M	50B	3	0.0	✗	355	41M	239M	50B	4	0.0	✗
356	41M	239M	50B	8	0.0	✗	357	41M	239M	50B	16	0.0	✗
358	476M	1301M	10B	10	0.2	✓	359	476M	2404M	10B	10	0.2	✓
360	476M	4604M	10B	10	0.2	✓	361	476M	9008M	10B	10	0.2	✓
362	476M	1301M	20B	10	0.2	✓	363	476M	2404M	20B	10	0.2	✓
364	476M	4604M	20B	10	0.2	✓	365	476M	9008M	20B	10	0.2	✓
366	476M	1301M	50B	10	0.2	✓	367	476M	2404M	50B	10	0.2	✓
368	476M	4604M	50B	10	0.2	✓	369	476M	9008M	50B	10	0.2	✓
370	793M	3964M	10B	10	0.0	✓	371	793M	3964M	10B	10	0.1	✓
372	793M	3964M	10B	10	0.2	✓	373	793M	3964M	10B	10	0.3	✓
374	793M	3964M	10B	10	0.4	✓	375	793M	3964M	10B	10	0.5	✓
376	793M	3964M	10B	10	0.6	✓	377	793M	3964M	10B	10	0.7	✓
378	793M	3964M	20B	10	0.0	✓	379	793M	3964M	20B	10	0.1	✓
380	793M	3964M	20B	10	0.2	✓	381	793M	3964M	20B	10	0.3	✓
382	793M	3964M	20B	10	0.4	✓	383	793M	3964M	20B	10	0.5	✓
384	793M	3964M	20B	10	0.6	✓	385	793M	3964M	20B	10	0.7	✓
386	793M	3964M	50B	10	0.0	✓	387	793M	3964M	50B	10	0.1	✓
388	793M	3964M	50B	10	0.2	✓	389	793M	3964M	50B	10	0.3	✓
390	793M	3964M	50B	10	0.4	✓	391	793M	3964M	50B	10	0.5	✓
392	793M	3964M	50B	10	0.6	✓	393	793M	3964M	50B	10	0.7	✓
394	1441M	7255M	10B	10	0.2	✓	395	1960M	7255M	10B	10	0.2	✓
396	2479M	7255M	10B	10	0.2	✓	397	3517M	7255M	10B	10	0.2	✓
398	6632M	7255M	10B	10	0.2	✓	399	1441M	7255M	20B	10	0.2	✓
400	1960M	7255M	20B	10	0.2	✓	401	2479M	7255M	20B	10	0.2	✓
402	3517M	7255M	20B	10	0.2	✓	403	6632M	7255M	20B	10	0.2	✓
404	1441M	7255M	50B	10	0.2	✓	405	1960M	7255M	50B	10	0.2	✓
406	2479M	7255M	50B	10	0.2	✓	407	3517M	7255M	50B	10	0.2	✓
408	6632M	7255M	50B	10	0.2	✓	409	453M	3964M	10B	2	0.5	✓
410	453M	3964M	10B	4	0.5	✓	411	453M	3964M	10B	6	0.5	✓
412	453M	3964M	10B	8	0.5	✓	413	453M	3964M	10B	10	0.5	✓
414	453M	3964M	10B	12	0.5	✓	415	453M	3964M	20B	2	0.5	✓
416	453M	3964M	20B	4	0.5	✓	417	453M	3964M	20B	6	0.5	✓
418	453M	3964M	20B	8	0.5	✓	419	453M	3964M	20B	10	0.5	✓
420	453M	3964M	20B	12	0.5	✓	421	453M	3964M	50B	2	0.5	✓
422	453M	3964M	50B	4	0.5	✓	423	453M	3964M	50B	6	0.5	✓
424	453M	3964M	50B	8	0.5	✓	425	453M	3964M	50B	10	0.5	✓
426	453M	3964M	50B	12	0.5	✓	427	566M	3964M	10B	3	0.33	✓
428	566M	3964M	10B	6	0.33	✓	429	566M	3964M	10B	9	0.33	✓
430	566M	3964M	10B	12	0.33	✓	431	566M	3964M	20B	3	0.33	✓
432	566M	3964M	20B	6	0.33	✓	433	566M	3964M	20B	9	0.33	✓
434	566M	3964M	20B	12	0.33	✓	435	566M	3964M	50B	3	0.33	✓
436	566M	3964M	50B	6	0.33	✓	437	566M	3964M	50B	9	0.33	✓
438	566M	3964M	50B	12	0.33	✓	439	476M	2404M	10B	2.5	0.2	✓
440	476M	2404M	20B	2.5	0.2	✓	441	476M	2404M	50B	2.5	0.2	✓
442	793M	3964M	100B	10	0.2	✓	443	476M	2404M	10B	20	0.2	✓
444	476M	2404M	20B	20	0.2	✓	445	476M	2404M	50B	20	0.2	✓
446	3070M	30249M	50B	20	0.2	✓	447	181M	907M	10B	40	0.2	✓
448	181M	907M	20B	40	0.2	✓	449	181M	907M	50B	40	0.2	✓

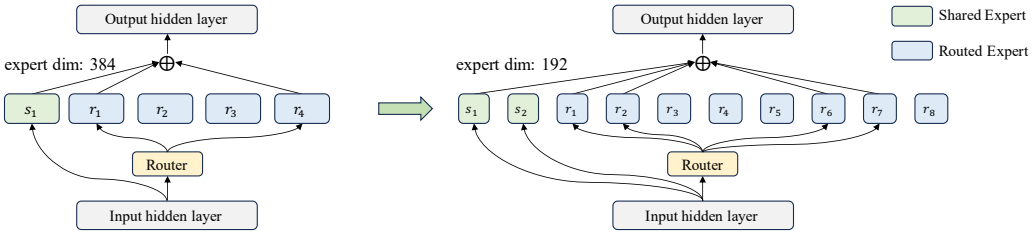

(a) Illustration of the variation of G.

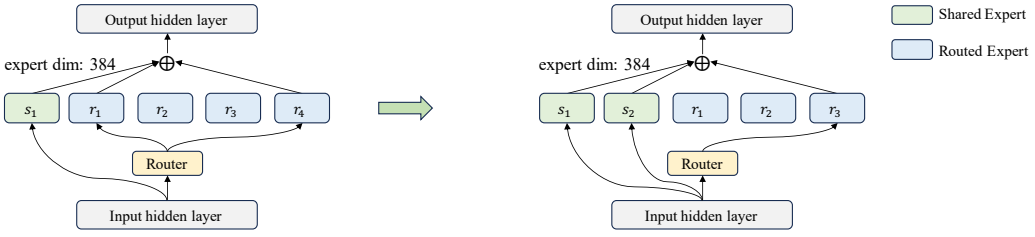

(b) Illustration of the variation of S.

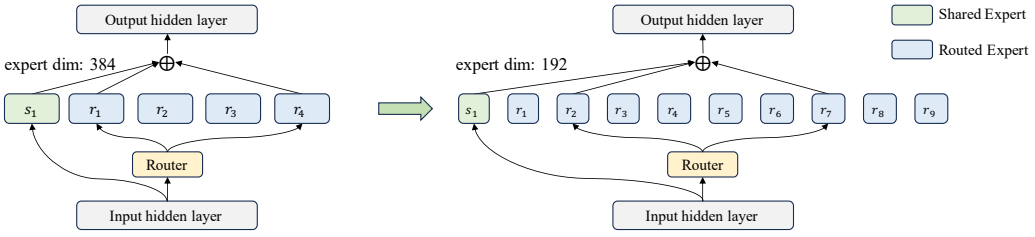

(c) Illustration of the variation of N_a.

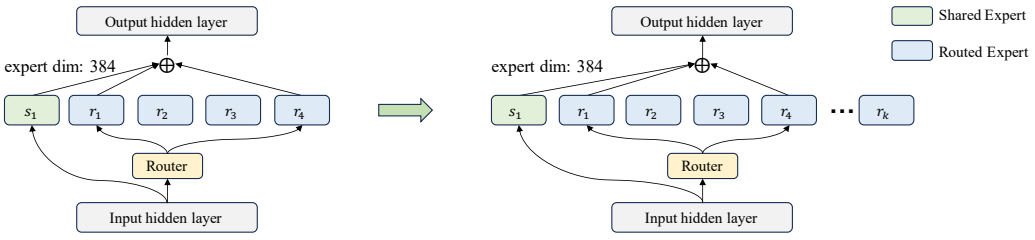

(d) Illustration of the variation of N.

Figure 17: Illustration of the variation of factor G, S, N_a and N under controlled conditions.

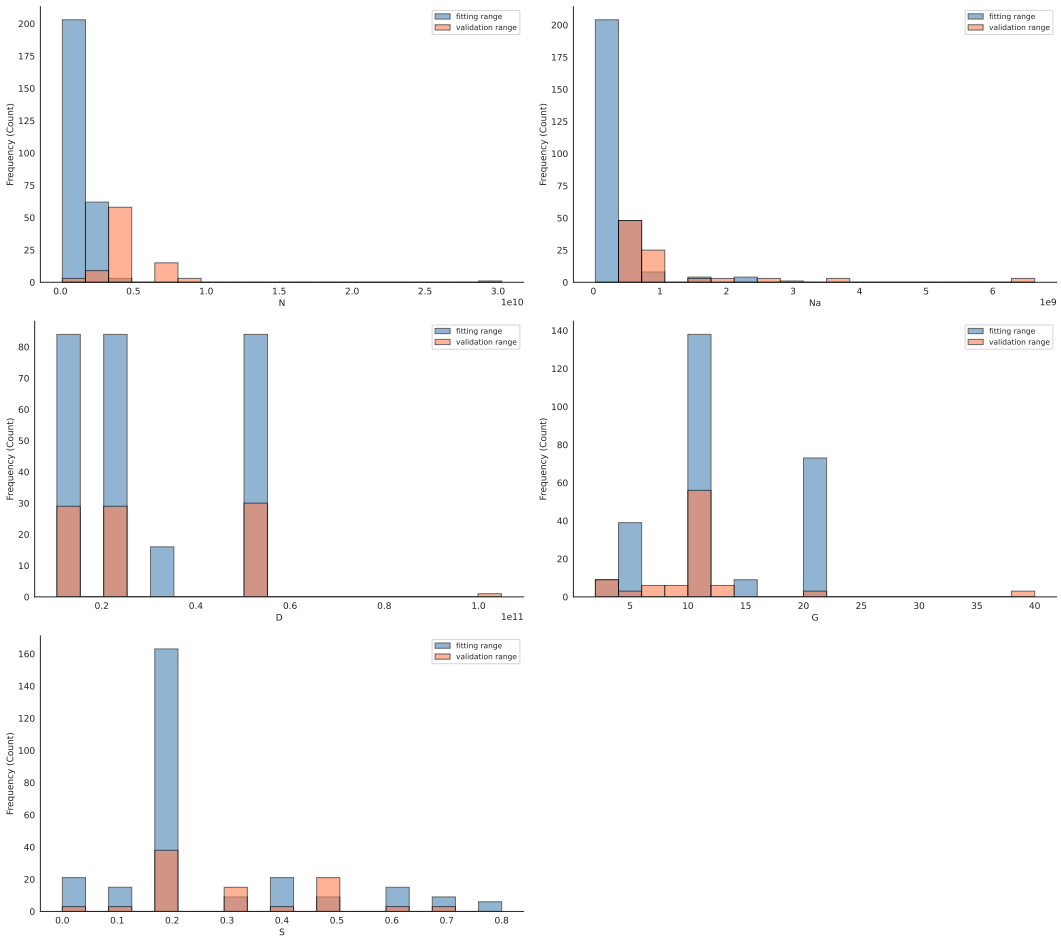

Figure 18: Distribution histograms of N, N_a, D, G, and S for fitting data and validation data.